Title
ANALYSIS OF THE DISINTEGRATION PRODUCTS FROM THE REACTIONS OF 125 MEV DEUTEROHS WITH LITHIUM NUCLEI

Author
Gilbert, Francis C.

Publication Date
1954-10-15

UCRL 2771

UNIVERSITY OF CALIFORNIA

Radiation Laboratory

BERKELEY, CALIFORNIA

DISCLAIMER

UCRL-2771
Unclassified Physics

UNIVERSITY OF CALIFORNIA
Radiation Laboratory
Berkeley, California

Contract No. W-7405-eng-48

ANALYSIS OF THE DISINTEGRATION PRODUCTS FROM THE REACTIONS OF 125-Mev DEUTERONS WITH LITHIUM NUCLEI

Francis C. Gilbert

(Thesis)

October 15, 1954

Printed for the U.S. Atomic Energy Commission

DISINTEGRATION PRODUCTS FROM 125-Mev DEUTERONS ON Li

Contents

ANALYSIS OF THE DISINTEGRATION PRODUCTS FROM THE REACTIONS OF 125-Mev DEUTERONS WITH LITHIUM NUCLEI

Francis C. Gilbert

Radiation Laboratory, Department of Physics
University of California, Berkeley, California

October 15, 1954

ABSTRACT

A thin lithium target(92.5% Li^7, 7.5% Li^6)was bombarded with the internal deuteron beam of the 184-inch cyclotron. The resulting fragments were detected in a row of nuclear track plates placed along a radial line from the target. An analysis of the tracks in the emulsions yielded the following information:

(a) energy distributions for the production of various fragments from 0^o to 70^o from the beam direction;

(b) the angular distribution of Li^8 nuclei in the reaction $H^2 + Li^7 \rightarrow H^1 + Li^8$;

(c) the range distribution of the alpha particles following the decays of Li^8 and B^8;

(d) the electron pickup by Li^8 ions as a function of their velocity;

(e) the range of Li^8 nuclei in emulsion.

In addition, absolute cross sections were obtained for processes (a) and (b) by means of exposures in the monitored external beam of the cyclotron.

ANALYSIS OF THE DISINTEGRATION PRODUCTS FROM THE REACTIONS OF 125-Mev DEUTERONS WITH LITHIUM NUCLEI

Francis C. Gilbert

Radiation Laboratory, Department of Physics
University of California, Berkeley, California

October 15, 1954

I. INTRODUCTION

During the past few years several experimenters have used the internal beam of the 184-inch cyclotron and nuclear track emulsion to study the high-energy disintegration of various elements by various particles. This type of experiment was first shown to be possible by Barkas and Bowker.[1] In this first experiment, the spallation fragments of $H\rho \approx 1.8 \times 10^5$ gauss-inch leaving a one-mil polystyrene target bombarded by 330-Mev protons were brought to a 180^o focus in the cyclotron magnetic field and were there detected by nuclear emulsion. By measuring the ranges in emulsion of the fragments Barkas and Bowker were able to identify and give the relative abundances of H^1, H^2, H^3, He^3, He^4, a group consisting of Li^6 and Be^7, and a group consisting of He^6 and Li^7.

It was then realized that this type of experiment would supplement nicely the data compiled by nuclear chemists on spallation reactions and by physicists on emulsion stars. Much excellent work[2-6] has been done radiochemically to determine the frequency distribution of residual nuclei remaining in cyclotron targets after high-energy bombardment. The great disadvantage of the radiochemical method is that it tells very little about the actual collision process within the nucleus. The distribution of residual nuclei seems to be determined principally by the shape of the nuclear potential valley in the region of the bombarded element. This suggests that after the initial disruption, the excited nucleus returns to the stable valley by an evaporation process, which is controlled mainly by the position of the excited nucleus with respect to the line of stable elements.

High-energy nuclear disintegrations initiated within the emulsion itself, both by cosmic rays[7-15] and by artificial beams,[16-17-18], have

been extensively studied. The distributions of range and angle of the star prongs have been measured and compared with theory. The observations to date suggest that the disintegration takes place in two steps: a nucleonic cascade[19, 20, 21] followed by a slower evaporation[22-25]. In the cascade process the incident nucleon is assumed to interact with one of the nucleons near the surface of the nucleus, the interaction being "similar" to that between free nucleons. If the energy imparted to the second nucleon is sufficient to raise it above the Fermi energy, it and the incident nucleon both continue through the nucleus to cause further interactions. In this way a cascade is built up which removes a few nucleons and considerable energy from this nuclear system. Some of the struck nucleons, however, have insufficient energy to escape, and thus the nucleus may still be left with sufficient excitation energy for evaporation to take place. The cascade process is completed in a time of the order of 10^{-22} second, and by 10^{-21} second the nucleus should be in thermal equilibrium and evaporating. These assumptions are supported by cosmic ray stars found in nuclear track emulsion which have the following general properties corresponding to the above suppositions: (a) a spectrum of "thin" (fast) tracks in the forward direction, mostly mesons, which are produced in the high-energy nucleon-nucleon collisions; (b) a spherically symmetric spectrum of "black" (slow) tracks which are the evaporation particles; and (c) a spectrum of "grey" tracks, somewhat collimated in the forward direction, which are the cascade protons. The analysis of stars in emulsion is complicated, however, by the presence of several types of nuclei in the emulsion, and by the difficulties of identifying and measuring the energies of both the primary and secondary particles.

To meet these difficulties, Barkas et al.[26] expanded their original apparatus to include three momentum positions for disintegration products in the forward direction. Polystyrene and beryllium targets were bombarded with 330-Mev protons, and the relative abundances and momentum distributions of the disintegration products were analyzed.

Thereafter Deutsch completed a more comprehensive survey experiment[27] in which he bombarded foils of Be, Al, Ni, Ag, Au, and U with 375-Mev alphas, 332-Mev protons and 187-Mev deuterons. Secondary

particles emerging from the disintegration of the nucleus at 0^{o} to the incident-beam direction were detected at three momenta, corresponding to alpha or proton energies of 6, 10, and 20 Mev. He also measured the angular distribution of fragments for 240-Mev alpha bombardment of Be, Al, Ni, and Ag. Here, secondary particles emitted at 0^{o}, 45^{o}, and 135^{o} were detected in nuclear emulsions at positions for which the secondary-proton and alpha energy was 6 Mev. In addition Deutsch bombarded a silver target with deuterons and alphas and obtained particles in ten energy positions in the forward direction for protons and alphas ranging from 5 to 22 Mev.[28] In general, his results were consistent with the evaporation model as refined by Le Couteur[25] except that the yield of high-energy protons did not fall off as rapidly as predicted from an evaporation theory. This may be attributed to the presence of the cascade protons in the forward direction.

During the scanning of the emulsions exposed to disintegration fragments, several Li^{8} and B^{8} hammer tracks were found. In a separate experiment using the same apparatus as Deutsch, Barkas[29] established seven points on the Li^{8} range-energy curve and three points on the B^{8} range-energy curve in Ilford C-2 emulsion. Using hydrogen and helium isotopes found at the same $\overline{H\rho}$, and the range-energy relation set forth by Wilkins[30] for alphas in emulsion, he determined the extension of the ranges of the various ions caused by electron pickup.

It was realized, during the course of these experiments, that if the shielding that defines the orbit channels is eliminated altogether and the plates are placed contiguously along a radial line to the target, continuous angular and energy distributions can be obtained. (Fig. 1). Also it is evident that higher-momentum particles may be otained at angles other than 0^{o}. It should be pointed out, however, that the background problems are increased by the removal of the shielding and that the analysis of the plates is complicated by the presence of tracks entering the emulsion from more than one direction.

The experiment described here utilizes the arrangement represented in Fig. 1 to make the following measurements:

(a) the energy and angular distribution of the disintegration fragments from a lithium target bombarded by 125-Mev deuterons,

(b) the angular distribution of the Li^8 fragments from the two-body reaction $H^2 + Li^7 \rightarrow H^1 + Li^8$ for 125-Mev deuterons,

(c) the range distribution of the alpha particles following the decays of the mirror nuclei Li^8 and B^8,

(d) the electron pickup by Li^8 (+++) ions as a function of their velocity,

(e) the range of Li^8 nuclei in emulsion.

In addition, absolute cross sections are obtained for processes (a) and (b) by means of exposures in the monitored external beam of the cyclotron.

II. GENERAL EXPERIMENTAL PROCEDURE

A. Apparatus and Exposures

The apparatus developed for this type of experiment is mounted on a cart that can be rolled through an air lock into the tank of the 184-inch cyclotron. It is so arranged that the target, a small strip of foil, is placed perpendicular to the cyclotron beam, and a series of strips of nuclear emulsion is set up on the same radial line of the cyclotron as the target, but about 4 inches below the level of the target (Fig. 1). Secondary fragments emerging from the target are deflected by the magnetic field of the cyclotron, those of lowest energy, being most greatly deflected, and the highest-energy particles going to the emulsions farthest from the target.

All the data, used in this report, with the exception of the measurement of absolute cross section(see Section II-D), were taken from nuclear track emulsion exposed, as described above. The target was a thin ribbon of lithium about 1/8 inch wide and a few mils thick stretched parallel to the magnetic field, with its smallest dimension perpendicular to the beam (Figs. 1, 2). The disintegration fragments then spiraled down to enter the emulsion surface at a grazing angle. Seven plates were used, extending from 10 inches to 32 inches from the target. Brass shielding protected the emulsions from the beam direction and from the cyclotron center.

It was found necessary to place an aluminum light shield about an inch above the plates and extending about 2-1/2 inches out from the shielding in order to reduce the intensity of background light in the cyclotron tank (Fig. 2). It was this light shield that limited the maximum projected angle β between the incident nucleon and the secondary fragment to about 60° for the nearest plate or about 80° for the farthest plate. The apparatus in position in the cyclotron cart is shown in Fig. 2a with the light shield in place, and in Fig. 2b without the light shield. In order to further reduce light intensity, the glass ports into the vacuum tank were covered, the tank pressure was kept low to minimize arcing, and the filament in the ion source was kept off except during the exposure. The beam was clipped vertically so that it was about 1 inch high, centered about 3 inches above the lip of the cart. At a radius about 2 inches great-

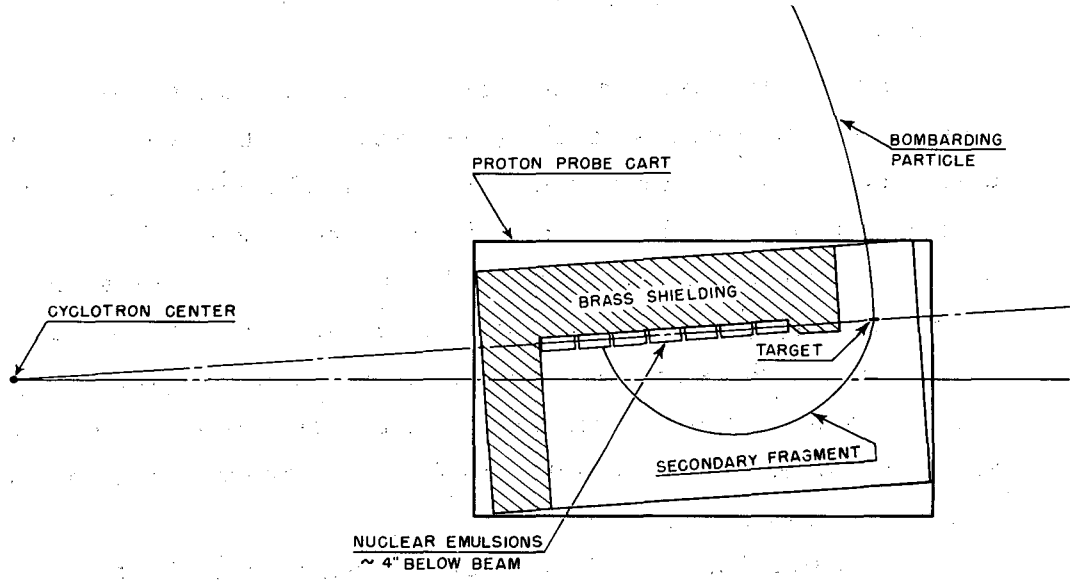

PLAN OF APPARATUS INSIDE CYCLOTRON.

MU-5100

Fig. 1 A plan view of the apparatus inside the cyclotron vacuum tank, showing typical orbits for a bombarding particle and a resulting fragment.

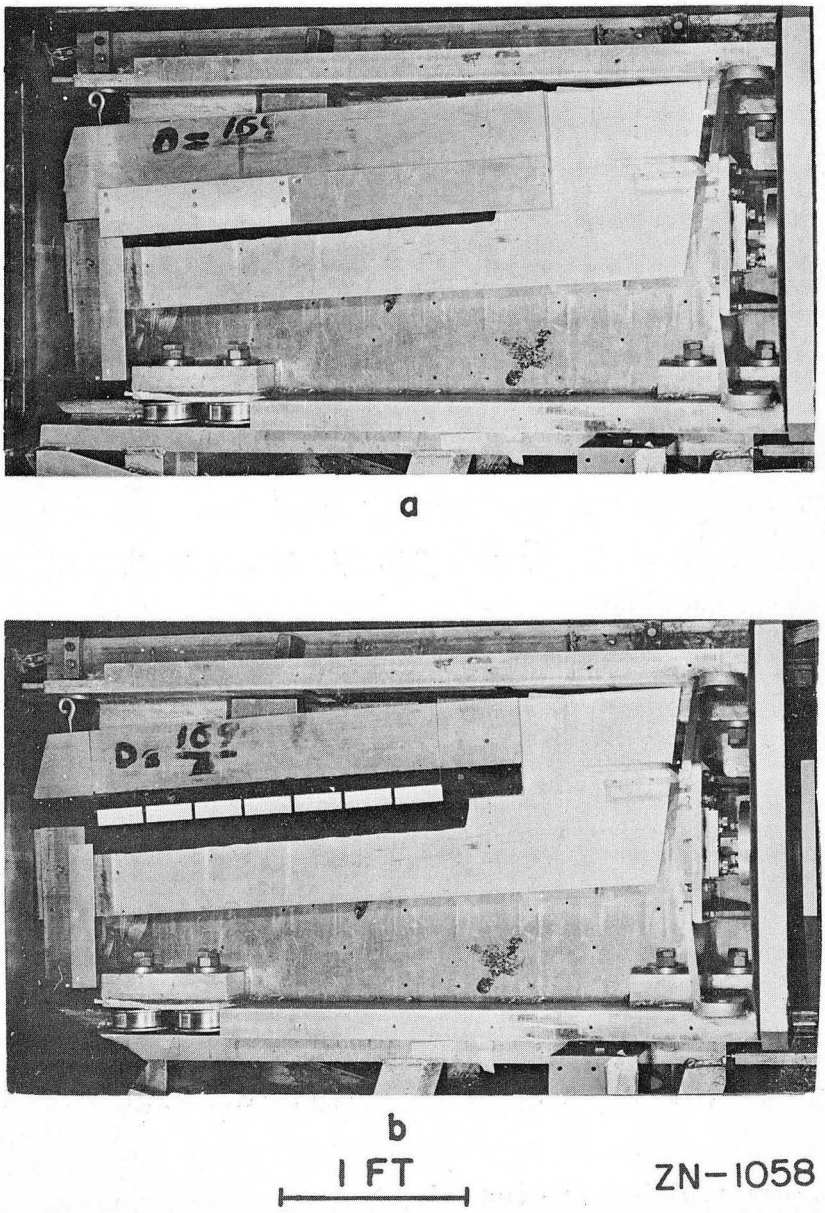

Fig. 2 Apparatus in cyclotron cart, (a) with light shield, (b) without light shield, showing seven plates in place.

er than the target radius the beam was absorbed by a carbon block on the far side of the cyclotron from the plates. At full beam current ($\sim 10^{-7}$ amperes) and with targets of the order of a mil in thickness, the optimum running times were about 10 seconds.

B. Method of Identification of Secondary Fragments

The identification of the fragments was made by a comparison of their ranges in emulsion with their momenta as determined from the radii of curvature of their paths in the cyclotron magnetic field. An expression for the $H\rho$ of a particle moving in the median plane of the non-uniform field of the cyclotron has been derived by Barkas[31] (Appendix C). This expression, in which the trajectories are described in cylindrical coordinates (r, ϕ, z), and which is corrected for an orbit lying slightly outside the median plane, is

$$\overline{H\rho} \approx \frac{\sec \gamma \int_{r_1}^{r_2} H(r)\, r\, dr}{r_1 \cos \beta_1 - r_2 \cos \beta_2}, \qquad (1)$$

where the subscripts refer to any two points on the orbit, $\tan \beta$ is $\frac{1}{r} \frac{dr}{d\phi}$, and γ is the angle of pitch of the spiral path. For the special case in consideration, where the initial and final points of the orbit lie on the same radial line, $\beta_2 \approx \pi - \beta_1$, (this approximation is good to $< 1\ 1/2$ degree in the region of the field used) and

$$\overline{H\rho} \cos \beta_2 \approx - \frac{\sec \gamma \int_{r_1}^{r_2} H(r)\, r\, dr}{r_1 + r_2}. \qquad (2)$$

$H(r)$ has been measured for the cyclotron magnetic field to an accuracy of 0.1%, and the function $\int_{r_1}^{r_2} H(r)\, r\, dr / (r_1 + r_2)$ has been calculated by numerical integration.[32]

The range-energy relations used for identification purposes were calculated from those of Wilkins[30] for protons and alpha particles in emulsion. Particles were considered identified if their ranges fell within 10% of the calculated loci. The figure 10% was chosen to cover the large straggle that occurs in $\overline{H\rho}$ for large values of the angle β ($\overline{H\rho}$ be-

ing proportional to sec β_1). In practice $\overline{H\rho}$ is determined from the quantity $\overline{H\rho} \cos \beta_2$ (Eq. 2) by dividing by the cosine of the horizontal projection of the angle between the beam and the fragment. This angle is also the angle between the short edge of the plate and the direction of the fragment where it enters the emulsion surface (Fig. 3).

All the light hydrogen and helium isotopes are readily separated except for H^2 and He^3, whose loci fall nearly together. Except for short ranges, however, these two nuclei can be distinguished by the difference in their grain or gap density. Li^6, Be^7, and B^8 also form a group, from which B^8 may be distinguished by its characteristic hammer track (see Section III-C). Of the other semistable nuclei ($\tau > 10^{-14}$ sec) with mass less than 9, Li^7 and He^6 fall together and Li^8 is identifiable by its hammer track.

Tracks that did not fall into the above categories were classed together as background. The background on the seven plates was fairly constant at about 7% but its character changed from plate to plate. On Position 1, about 75% of the background consisted of short tracks that were too short to identify, and which probably were fragments that had picked up an electron or more in the target. This short-range background decreased to about 10% of the total background on Position 7. It was replaced at these higher energies by a random background of particles that were diving too steeply to have come from the target. I believe this latter background to be caused by secondary fragments produced in the aluminum light shield above the plates by deuterons (in the beam) with large vertical oscillations. There was also a fairly constant (~2%) background of tracks that were not diving too steeply to have come from the target. I believe that these came from the target holder and other objects near the target, which were hit by a part of the beam that was scattered off the vertical and radial beam clippers.

C. Method of Data Reduction

The quantities that are measured in scanning the nuclear emulsion for disintegration products are

(a) the ranges R of the tracks,

(b) the angles β (see Fig. 3),

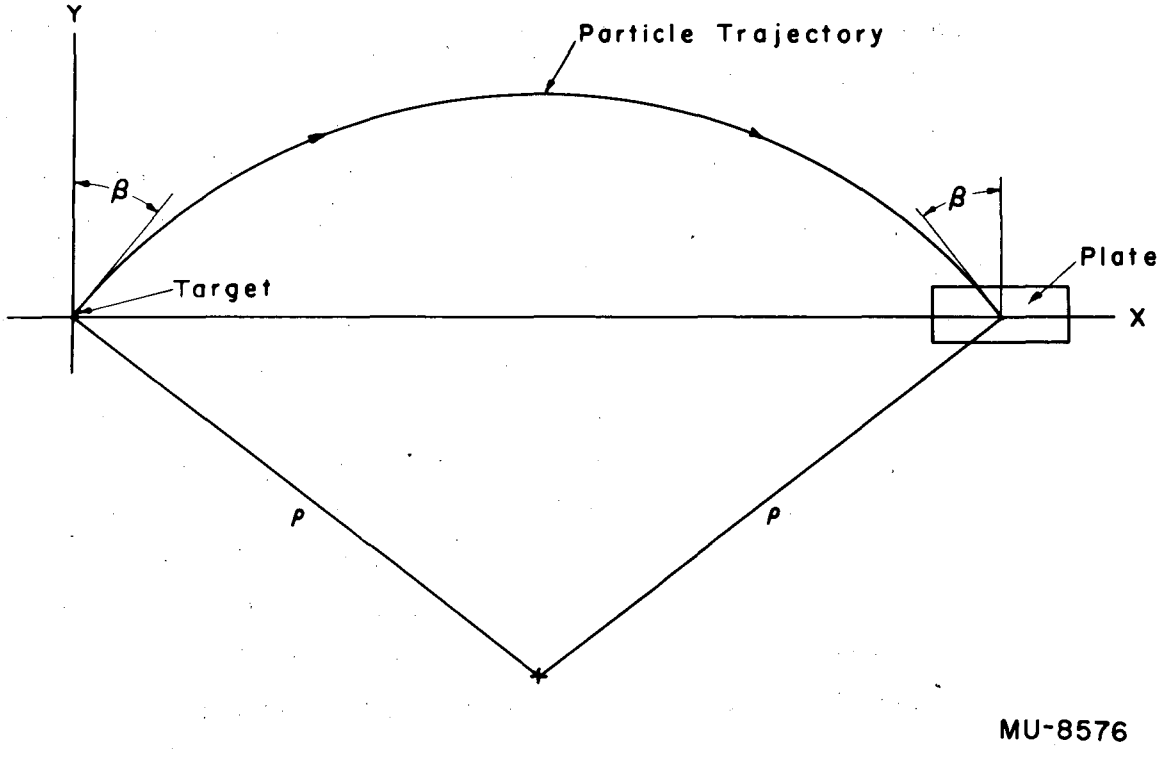

Fig. 3 The positions of the target, plate and particle trajectory are shown in terms of the coordinates used in the text. For the purpose of this illustration the field is assumed uniform.

(c) the coordinates (x, y),

(d) the area A scanned to find N tracks.

The identification to give the charge qe and the mass M of the fragment is made from (a), (b), and (c) above as described in the previous section. It is then necessary to convert the number of events N found in area A and angular interval $\Delta\beta$ to the number of events N leaving the target in the solid angle $\Delta\omega$ and the momentum interval Δp. Barkas[33] has derived a convenient expression for this transformation, which in terms of these variables is

$$\frac{N}{\Delta\omega\Delta p} = \frac{2zc\cos^2\beta}{Hqe}\left[1 + \frac{x^2\left(\frac{\pi}{2} - \beta\right)^2}{z^2\cos^2\beta}\right] x \frac{N}{A\Delta\beta}, \qquad (3)$$

where H is the magnetic field intensity and z is the coordinate parallel to the magnetic field and perpendicular to the plane of Fig. 3. For a description of this derivation see Appendix D. This expression assumes a uniform magnetic field. The known nonuniformity of the field causes Eq. 3 to be in error by less than 2%.

In this experiment I have expressed the results in terms of energy intervals rather than momentum intervals. From the relation $E^2 = p^2c^2 + m^2c^4$ we obtain

$$\frac{dT}{dp} = \frac{dE}{dp} = v \approx \frac{p}{M} = \frac{qe\overline{H\rho}}{cM},$$

where T is the kinetic energy. The final expression then becomes

$$\frac{N}{\Delta\omega\Delta T} = \frac{2Mzc^2\cos^2\beta}{H(\overline{H\rho})q^2e^2}\left[1 + \frac{x^2\left(\frac{\pi}{2} - \beta\right)^2}{z^2\cos^2\beta}\right] x \frac{N}{A\Delta\beta}. \qquad (4)$$

On each position the data have been divided into angular intervals, $\Delta\beta = \beta_2 - \beta_1$, of magnitude 5°, and transformed by the above equation, which was evaluated at $\bar{\beta} = \frac{\beta_1 + \beta_2}{2}$. When data from several angular intervals were combined (as in Sections III A, B, and D), I used the form $\sum_i N_i / \sum_i \Delta\omega_i \Delta T_i$. (5)

The kinetic energies of the fragments were determined from

$$T = \frac{p^2}{2M} = \frac{(qH\rho)^2}{2Mc^2} ,$$

except for the protons, for which the relativistic expression

$$T = \sqrt{p^2 c^2 + M^2 c^4} - Mc^2$$

was used. For any particular angular interval $\beta_2 - \beta_1$, shown in Figs. 7 through 11, the spread in energy, $T_2 - T_1$, was determined from β_2 and β_1 by the above equations. The higher energy T_2 was increased by the energy loss corresponding to the target thickness at that angle.

D. Determination of Absolute Cross Sections

The measurement of absolute cross sections for runs made inside the cyclotron tank is rendered difficult by the lack of a good method for determining the total amount of beam passing through the target. An attempt at monitoring the residual activity in the target has been made,* and seems promising for the heavy elements. The activity remaining in thin lithium targets, however, is insufficient for reliable counting methods. Therefore it was decided to repeat the exposure using the external cyclotron beam, which could be easily monitored with a Faraday cup. Although no magnetic field was used and consequently no separation of nuclei was feasible (with the exception of Li^8 and B^8), it was possible to obtain an absolute cross section for the production of fragments as a function of their residual range in emulsion. This cross section could then be broken down to give the probabilities for the production of various nuclei by using the relative cross sections obtained from the internal runs.

The experimental arrangement is shown in Figs. 4 and 5. The cyclotron beam was collimated to 1/4-inch by the 48-inch deuteron tube collimator. The target was placed in the center of the scattering chamber at 90^o to the beam direction. After the emulsions and target were placed in the chamber, it was pumped down by an auxiliary vacuum pump and then opened to the cyclotron vacuum. The position of the beam at the target was determined by exposing an x-ray film suspended on the target holder. The total exposure for a run was measured by passing the cur-

* Evan Bailey - private communication

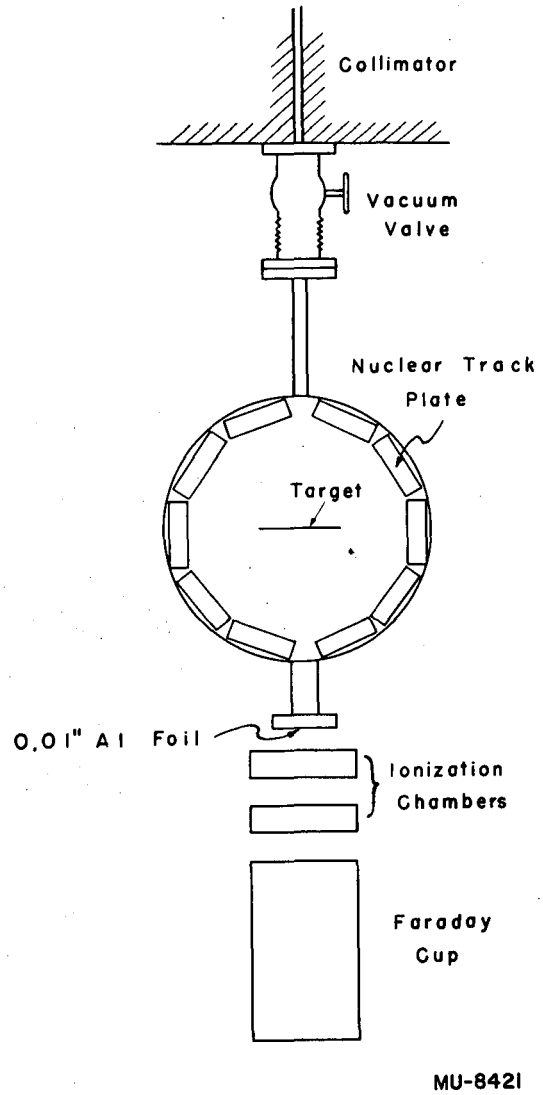

Fig. 4 A plan view of the experimental arrangement for the measurement of the absolute cross section, using the external cyclotron beam.

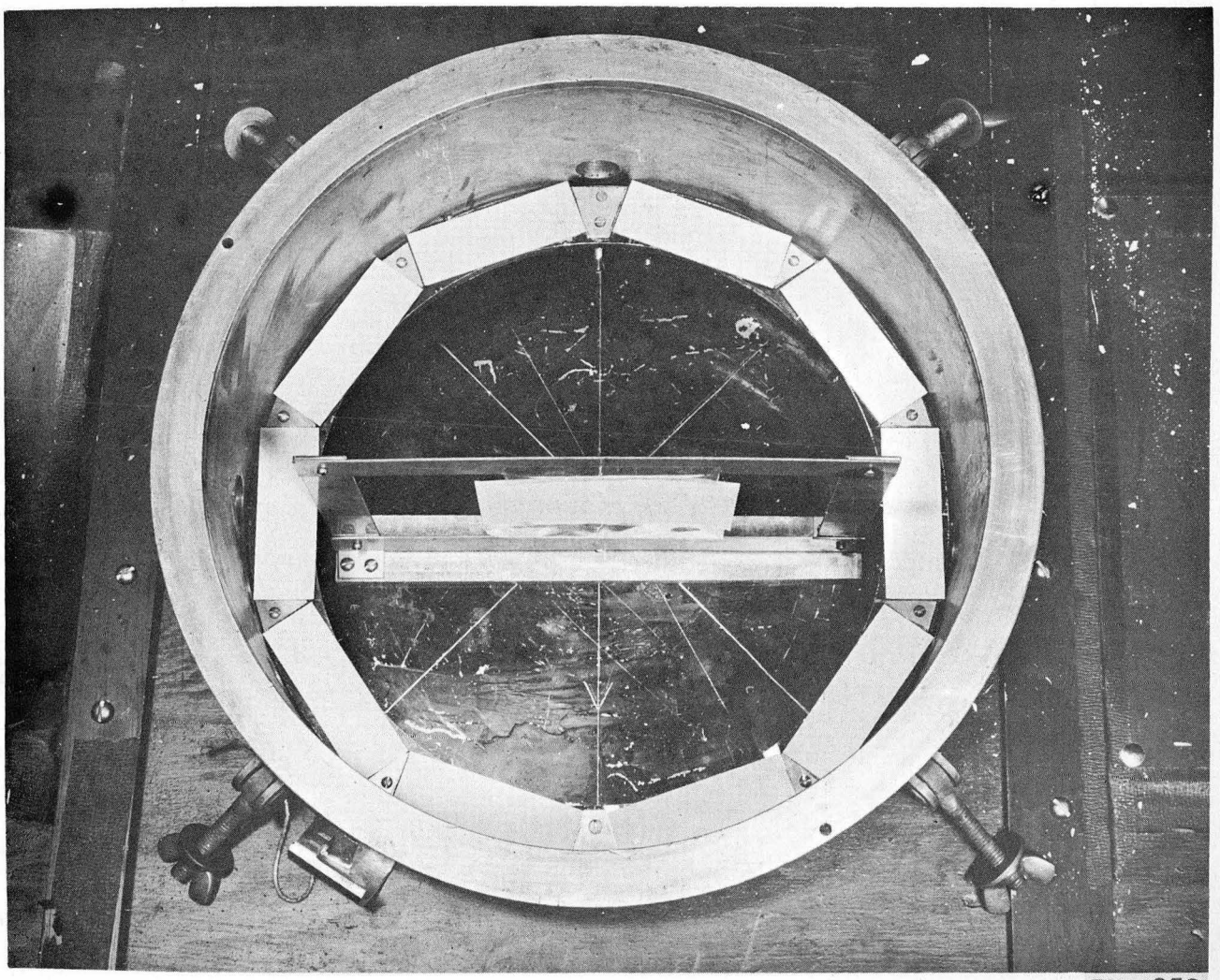

Fig. 5 The scattering chamber, with ten plates and a target in place.

rent from the Faraday cup into a calibrated capacitor whose charge was measured by a high-impedance electrometer. Of the two ionization chambers, one was used by the cyclotron crew for tuning purposes and the other was a calibrated chamber used to monitor low beams and to provide a rough check on the operation of the Faraday cup and its circuit.

The areal density of the lithium target (2.3 mg/cm^2) was determined by measuring its area and by weighing the lithium sulphate formed when it was dissolved in dilute sulphuric acid. The preparation and handling of the lithium targets are explained in Section II-A.

External runs were made at both 190 and 147 Mev. (The lower energy was obtained by passing the beam through one inch of aluminum.) The cross section for the production of fragments with ranges between 150 and 1000 microns was extrapolated from 147 Mev to 125 Mev, assuming a linear relation with energy. This extrapolation assumes an increase in the cross section by 6 1/2%, from 147 to 125 Mev.

In order to obtain an absolute cross section for the internal runs it is necessary to sum the number of particles with ranges between R_1 and R_2 in the internal run and compare this number with the number of tracks between R_1 and R_2 in the monitored external run. R_1 was chosen to be 150 microns, long compared with the equivalent target thickness of about 8 microns. R_2 was taken to be 1000 microns, short enough to prevent many particles from escaping through the bottom of the 200-micron emulsion (the dip angle was 6.5°). Figure 6 is a histogram in 50-micron intervals of the tracks from the external run at an angle θ of 58°. The solid curve represents $\sum_i \frac{\Delta N_i}{\Delta \omega_i \, \Delta T_i} \left(\frac{dT}{dR}\right)_i$, where $\frac{\Delta N_i}{\Delta \omega_i \, \Delta T_i}$ is the relative cross section for producing particle i (H^1, H^2, ...etc.) internally, averaged between 55° and 65°, and $\left(\frac{dT}{dR}\right)_i$ is evaluated from Barkas and Young's table of emulsion functions [34]. The solid curve has been normalized so that its area between 150 and 1000 microns is equal to the number of events (97) found within those limits from the external run. By these measurements it was established that one particle per steradian per 50 microns from the internal run is equal to 8.1×10^{-32} cm^2 per steradian per 50 microns. I

have applied this factor to determine the absolute cross sections given in Sections III–A and III-B. I believe this ratio to be accurate to about 10%.

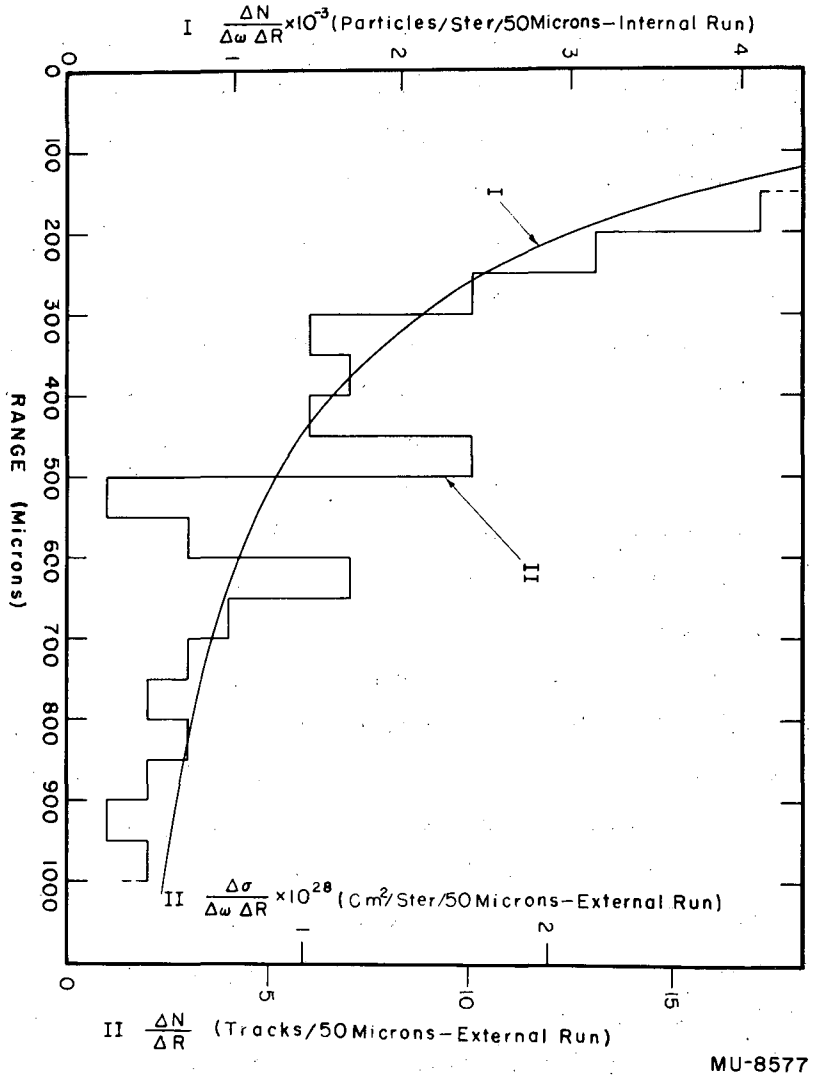

Fig. 6 Range distribution of the particles from the external run. The solid curve represents the smoothed sum of the various particles from the internal run normalized to the area of the histogram.

III RESULTS AND DISCUSSION

A. The Differential Cross Section for the Production of Secondary Fragments from the Disintegration of Lithium Nuclei by 125-Mev Deuterons.

A natural lithium target (92.5% Li^7, 7.5% Li^6, < 1% O^{16}; see Appendix A) was bombarded with deuterons at a radius of 65-inch in the 184-inch cyclotron. The resulting disintegration fragments were detected by seven nuclear track plates placed along a radial line from the target but below the cyclotron beam (Section II-A). The fragments were identified by their range-momentum relationships (Section II-B) and classified as follows: H^1, H^2, H^3, He^3, He^4, Li^6 - Be^7, He^6 - Li^7, Li^8, B^8, and a group consisting of background and unidentifiable particles. This last group constituted about 7% of the total tracks and is discussed in section II-B. The data were combined (see Section II-C) to give the differential cross section (per Mev per steradian) for the production of a specific fragment, averaged from 0° to 30°, 30° to 50°, 50° to 60°, and 60° to 70°. The results are tabulated in Table I. For H^1, H^2, H^3, He^3, and He^4, for which the statistics are the best, the results are plotted in Fig. 7 through 11.

The energy range seen by the seven plates is, of course, a function of the angle β. Thus for protons at 0° the energy range covered by the seven plates is 2.1 to 15.7 Mev, while at 70° it is 18.0 to 134 Mev. The C-2 emulsion used was not sensitive enough, however, to reliably detect protons above 80 Mev. The errors shown on the cross sections are statistical. The energy shown is the average of the energy range (given in Table I) represented by that point, including an allowance for target thickness (equivalent to 8 microns in emulsion). No values are given in Table I for the cross section for particles between 60° and 70° on Position 1. The light shield placed above the emulsions (see Fig. 2) eliminated the particles greater than 60° on Position 1, and perhaps interfered with those in the range from 50° - 60° in this one position.

Table I

The number of particles, the average cross section, and the average energy for the various fragments from the disintegration of lithium nuclei by 125-Mev deuterons, averaged over the angles indicated.

Position	0° - 30°			30° - 50°			50° - 60°			60° - 70°		
	N[a]	$\frac{\Delta\sigma}{\Delta\omega\Delta T}$[b]	T_1 and T_2[c]	N	$\frac{\Delta\sigma}{\Delta\omega\Delta T}$	T_1 and T_2	N	$\frac{\Delta\sigma}{\Delta\omega\Delta T}$	T_1 and T_2	N	$\frac{\Delta\sigma}{\Delta\omega\Delta T}$	T_1 and T_2
					H^1							
1	129	2.28	2.1, 3.0	127	1.57	2.8, 5.0	6	1.06	5.0, 8.2			
2	87	2.24	3.5, 4.8	82	1.48	4.6, 8.4	67	1.06	8.4, 13.8	74	0.426	13.8, 29.5
3	99	2.00	5.2, 7.0	96	1.44	7.0, 12.6	69	0.852	12.6, 20.8	85	0.387	20.8, 44.4
4	125	1.93	7.3, 9.7	99	1.17	9.7, 17.6	79	0.748	17.6, 29.0	83	0.281	29.0, 62.0
5	132	1.90	9.8, 13.1	126	1.35	13.1, 23.7	80	0.676	23.7, 39.2	56	0.177	39.2, 83.8
6	143	1.90	12.5, 16.7	133	1.17	16.7, 30.3	81	0.559	30.3, 50.0	41	0.104	50.0, 107
7	179	1.86	15.8, 21.1	173	1.14	21.1, 38.3	81	0.413	38.3, 63.2	20	(0.118)	63.2, 135
					H^2							
1	73	(2.57)	1.0, 1.6	66	(1.62)	1.4, 2.8	1	(0.350)	2.5, 4.4			
2	50	(2.58)	1.7, 2.6	29	(1.05)	2.3, 4.4	35	1.11	4.2, 7.1	8	0.922	6.9, 14.7
3	26	(1.06)	2.6, 3.8	34	1.03	3.5, 6.5	32	0.788	6.3, 10.4	25	2.25	10.4, 22.2
4	36	(1.11)	3.6, 7.1	57	1.34	4.9, 8.8	27	0.507	8.8, 14.5	19	0.130	14.5, 31.0
5	53	1.53	4.9, 6.7	44	0.962	6.6, 11.8	26	0.432	11.8, 19.6	10	0.065	19.6, 41.9
6	61	1.62	6.2, 8.3	47	0.829	8.3, 15.1	22	0.298	15.1, 25.0	7	0.035	25.0, 53.5
7	71	1.48	7.9, 10.5	57	0.739	10.5, 19.1	27	0.270	19.1, 31.6	11	0.405	31.6, 67.5

H^3

1	18	(0.977)	0.7, 1.6	49	1.83	0.9, 2.2	5	2.64	1.7, 3.1			
2	28	2.15	1.2, 2.2	38	2.04	1.5, 3.2	25	1.18	2.8, 4.9	14	0.242	4.6, 9.8
3	28	1.70	1.7, 2.7	36	1.59	2.3, 4.5	33	1.23	4.2, 7.1	37	0.501	6.9, 14.8
4	37	1.70	2.4, 3.6	36	1.27	3.2, 6.2	37	1.05	5.9, 9.6	24	0.245	9.6, 20.7
5	40	1.74	3.3, 4.7	47	1.53	4.4, 8.1	41	1.03	7.9, 13.1	29	0.262	13.1, 27.9
6	53	2.11	4.1, 5.9	61	1.62	5.6, 10.1	30	0.683	10.1, 16.7	22	0.164	16.7, 35.7
7	53	1.65	5.3, 7.2	67	1.31	7.0, 12.8	36	0.443	12.8, 21.1	9	0.492	2.1, 45.0

He^3

1	23	(0.307)	2.7, 4.9	29	(0.269)	3.6, 7.6	1	(0.133)	6.6, 11.6			
2	11	(0.213)	4.6, 7.2	22	(0.297)	6.1, 11.9	19	0.225	11.2, 18.9	6	0.260	18.4, 39.4
3	39	(0.591)	6.9, 10.0	41	0.447	9.3, 17.3	8	0.073	16.8, 27.8	5	0.017	27.8, 59.2
4	53	(0.614)	9.7, 13.5	25	0.222	12.9, 23.5	4	0.029	23.5, 38.7	0	0	38.7, 82.7
5	51	0.548	13.1, 18.0	17	0.138	17.5, 31.6	4	0.026	31.6, 52.3	0	0	52.3, 112
6	55	0.536	16.7, 22.3	13	0.083	22.3, 40.4	1	0.051	40.4, 66.7	0	0	66.7, 143
7	56	0.437	21.1, 28.2	14	0.068	28.2, 51.1	0	0	51.1, 84.3	0	0	84.3, 18.0

[a] number of events

[b] in millibarns/steradian/Mev

[c] energy range in Mev

Table I (cont'd)

Position	0° - 30°			30° - 50°			50° - 60°			60° - 70°		
	He^4											
	N[a]	$\frac{\Delta\sigma}{\Delta\omega\Delta T}$[b]	T_1 and T_2[c]	N	$\frac{\Delta\sigma}{\Delta\omega\Delta T}$	T_1 and T_2	N	$\frac{\Delta\sigma}{\Delta\omega\Delta T}$	T_1 and T_2	N	$\frac{\Delta\sigma}{\Delta\omega\Delta T}$	T_1 and T_2
1	200	(3.55)	2.1, 4.4	205	2.54	2.7, 6.3	4	0.704	5.0, 9.4			
2	133	3.35	3.4, 6.0	93	1.67	4.6, 9.4	47	0.745	8.4, 14.4	20	0.115	13.8, 29.5
3	119	2.42	5.2, 8.1	84	1.26	7.0, 13.3	27	0.332	12.6, 21.4	10	0.045	20.8, 44.4
4	125	1.93	7.2, 10.6	83	0.970	9.7, 18.2	29	0.274	17.6, 29.0	3	0.010	29.0, 62.0
5	127	1.85	9.8, 13.9	72	0.786	13.1, 24.2	11	0.092	23.7, 39.2	2	0.0062	39.2, 83.8
6	123	1.63	12.5, 17.3	53	0.525	16.7, 30.3	4	0.027	30.3, 50.0	0	0	50.0, 107
7	111	1.16	15.8, 21.6	40	0.262	21.1, 38.3	5	0.025	38.3, 63.2	0	0	63.2, 135
	Li^6 and Be^7											
1	5	0.059	3.1, 7.8	9	0.075	4.1, 11.1	6	0.071	7.4, 16.0			
2	8	0.138	5.2, 10.0	11	0.132	6.9, 15.3	8	0.083	12.6, 23.4	14	0.053	20.7, 46.4
3	7	0.094	7.8, 13.0	12	0.119	10.5, 21.0	1	0.0079	18.9, 33.3	5	0.015	31.2, 66.5
4	11	0.114	10.9, 16.6	10	0.079	14.6, 28.2	1	0.0063	26.4, 45.1	0	0	43.5, 93.0
5	9	0.085	14.7, 21.3	2	0.014	19.6, 37.0	0	0	35.6, 58.8	1	0.0021	58.8, 126
6	9	0.080	18.8, 26.4	0	0	25.0, 46.6	1	0.0046	45.4, 75.0	1	0.0017	75.0, 160
7	8	0.054	23.7, 32.9	1	0.0044	31.6, 57.5	0	0	57.5, 94.8	0	0	94.8, 202

	He^6				Li^7							
1	9	0.124	2.64, 8.0	11	0.106	3.51, 10.6	1	0.138	6.4, 15.0			
2	6	0.120	4.4 , 9.6	9	0.126	5.9 , 14.1	5	0.062	10.8, 21.0	3	0.014	17.8, 40.8
3	16	0.252	6.7 , 11.8	12	0.141	9.0 , 18.8	3	0.029	16.2, 29.4	5	0.017	26.8, 57.1
4	15	0.183	9.3 , 14.8	8	0.073	12.5 , 24.7	2	0.014	22.6, 39.3	0	0	37.3, 79.7
5	14	0.157	12.6 , 18.9	1	0.0079	16.8 , 32.2	0	0	30.4, 50.4	0	0	50.4, 108
6	7	0.072	16.1 , 23.0	4	0.028	21.5 , 40.5	1	0.0052	39.0, 64.4	1	0.0020	64.4, 138
7	2	0.016	20.3 , 28.8	3	0.015	27.2 , 49.3	0	0	49.3, 81.3	0	0	81.3, 174

[a] number of events

[b] in millibarns/steradian/Mev

[c] energy range in Mev

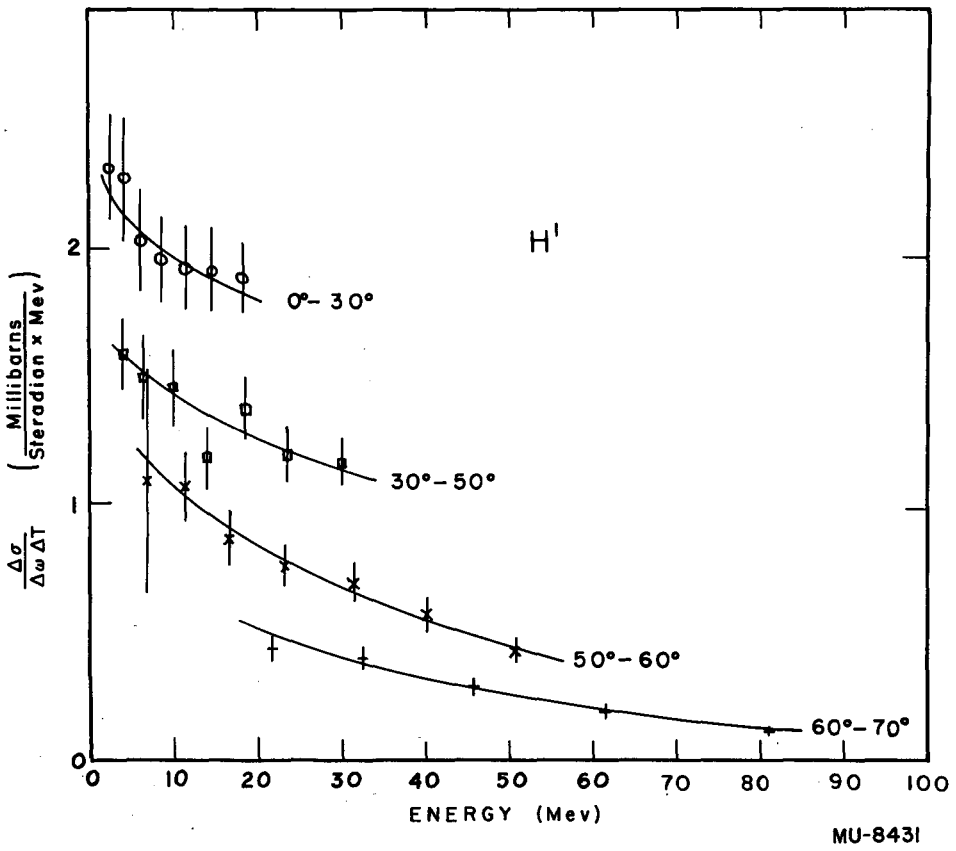

Fig. 7 The laboratory-system differential cross section for the production of H^1 from the disintegration of lithium nuclei by 125-Mev deuterons, averaged over the angles indicated. The errors shown are statistical only.

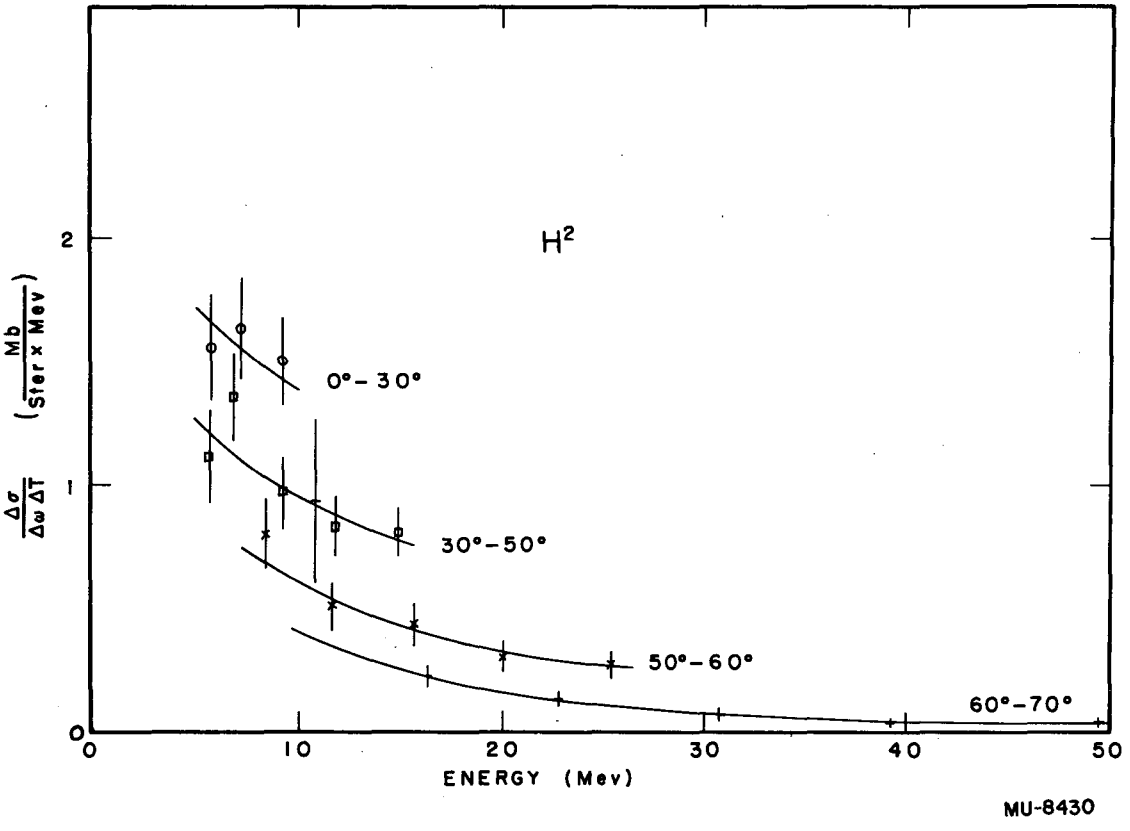

Fig. 8 The laboratory-system differential cross section for the production of H^2 from the disintegration of lithium nuclei by 125-Mev deuterons, averaged over the angles indicated. The errors shown are statistical only.

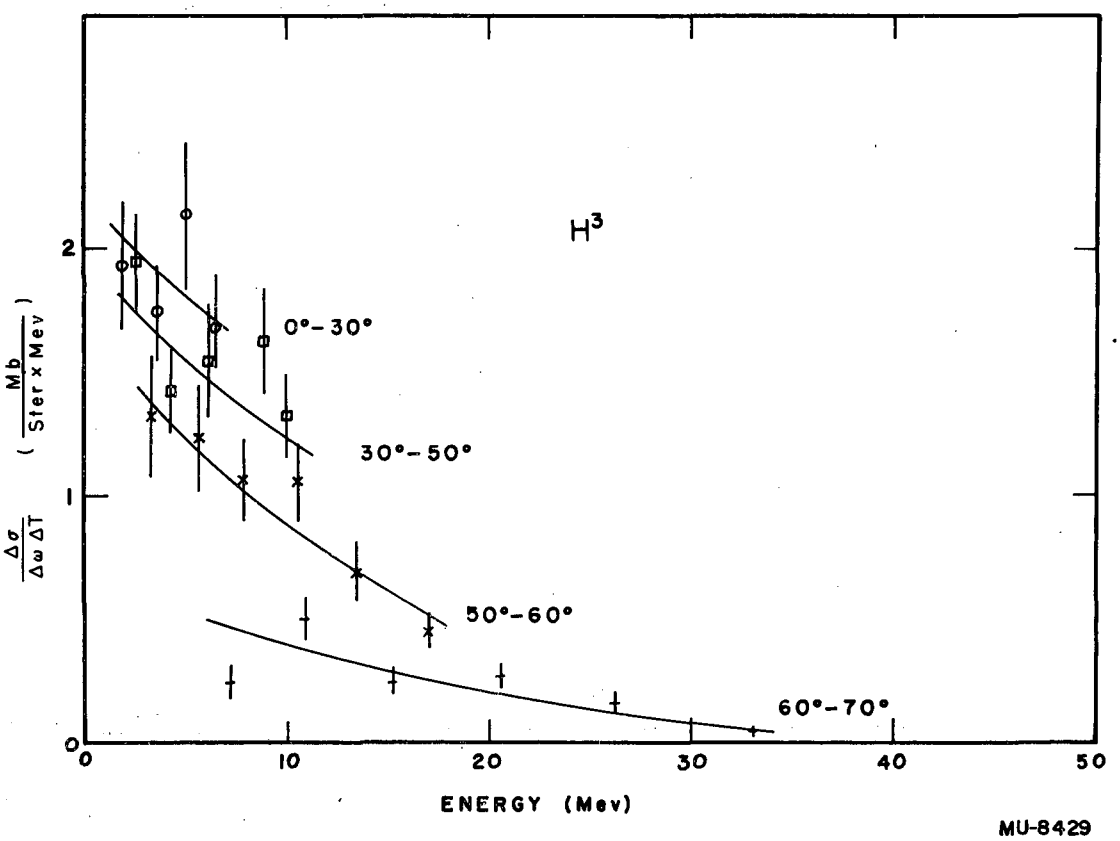

Fig. 9 The laboratory-system differential cross section for the production of H^3 from the disintegration of lithium nuclei by 125-Mev deuterons, averaged over the angles indicated. The errors shown are statistical only.

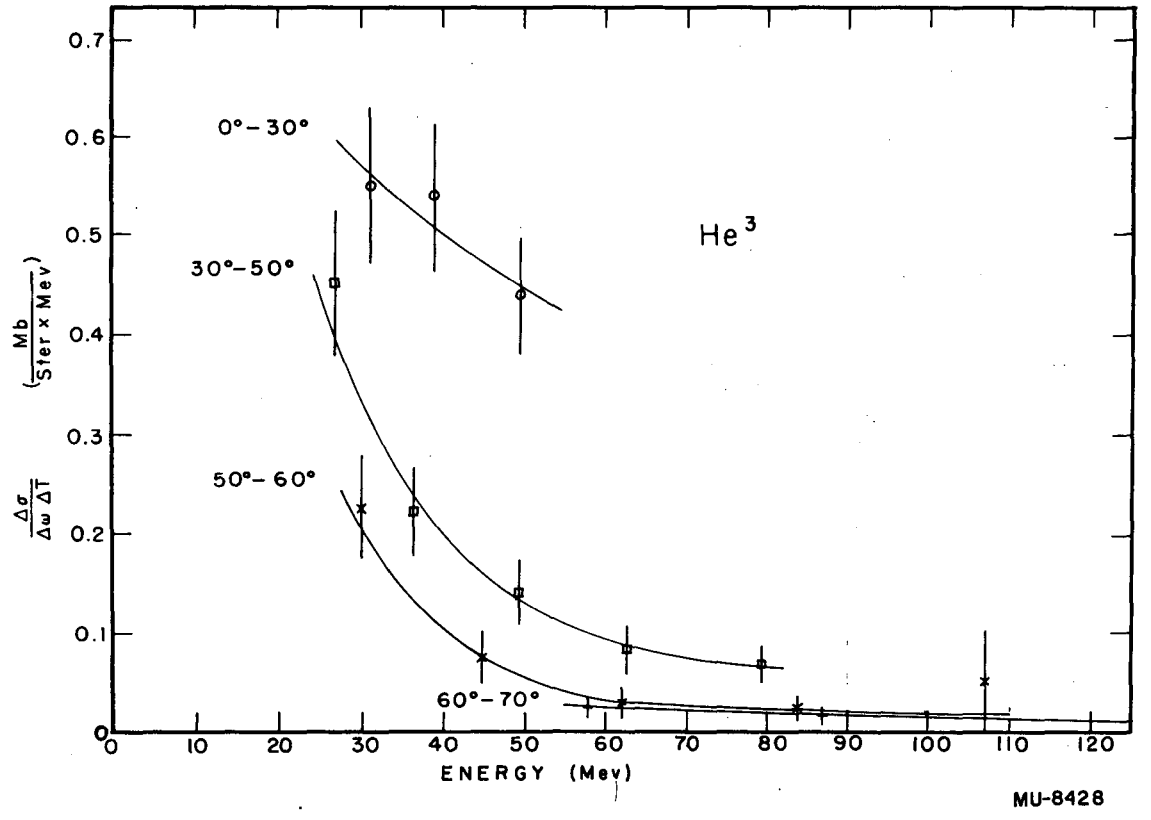

Fig. 10 The laboratory-system differential cross section for the production of He^3 from the disintegration of lithium nuclei by 125-Mev deuterons, averaged over the angles indicated. The errors shown are statistical only.

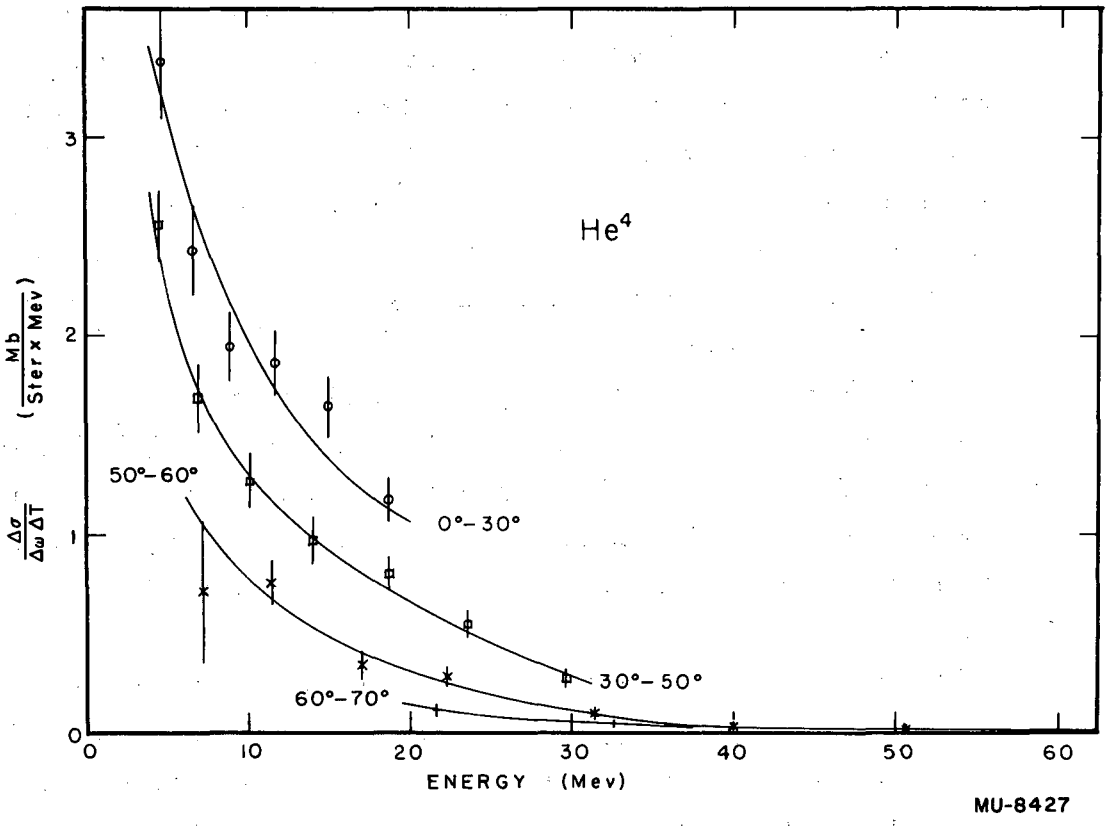

Fig. 11 The laboratory-system differential cross section for the production of He^4 from the disintegration of lithium nuclei by 125-Mev deuterons, averaged over the angles indicated. The errors shown are statistical only.

The scatter of the points for H^2 and He^3 at low energies might indicate that the discrimination between the two nuclei for short ranges is not so good as was anticipated. The two nuclei were distinguished on the basis of the appearance of the track (He^3 gives a heavier track for the same range than H^2). Because the emulsions were somewhat over-developed, the discrimination below 50 microns is questionable. The same observation applies to He^4 and H^3; however, the range difference between these two nuclei at the same $\overline{H\rho}$ is sufficient to separate them except at the lowest energy point (< 10 microns). In the light of these considerations and for easy visualization, I have drawn smooth curves through the points in Fig. 7 through 11 with shapes similar to those for the protons, and I have omitted the doubtful points listed above. (These doubtful points are included in Table I, however enclosed in brackets). It should be pointed out that the sum of the number of H^2 plus He^3 tracks and the sum of the number of H^3 and He^4 tracks at these low ranges are not affected by this lack of discrimination. In order to improve the statistics on some of the points shown in Fig. 9 for H^3, I have combined data from several plates.

Li^6 and Be^7 could not be separated and are combined in Table I. I have handled this group as if it were all Li^6. He^6 and Li^7 also are inseparable and I have treated this group as if it were all Li^7. These two groups are probably reduced semewhat at low energies owing to electron pickup in the target (Section III-D). Li^8 and B^8 are treated in Section III B.

It is difficult to analyze the data in terms of the usual nuclear models. There are too few nucleons present to use a statistical model such as the evaporation model of Weisskoff[22] or the cascade model of Goldberger[20], and too many nucleons to separate all the specific reactions, except for the reaction $H^2 + Li^7 \rightarrow H^1 + Li^8$ (see Section III-B). Some general observations can be made, nevertheless. It is first noted that all the fragments show a strong angular dependence, being peaked in the forward direction. Part of this angular distribution is due to the center-of-mass velocity. It is impossible, though, to pick a unique velocity such that the distributions are spherically symmetric in the center-of-mass

system for all energies. It is also apparent that the distributions are not of the Maxwellian form predicted by the evaporation theories for heavier elements,[22] i.e.,

$$P(T)\,dT = \frac{T - V}{\tau^2}\, e^{-\frac{T - V}{\tau}}\, dT \qquad (6)$$

where $P(T)$ is the probability of evaporating a particle with energy between T and $T + dT$, V is the potential barrier, and τ is the nuclear temperature.

The relative numbers of the various particles are not in agreement with the pickup process of Bransden,[35] which, for example, would predict approximately the same number of H^3 as He^3 particles. Actually the number of He^3 is about 1/3 that of H^3. The reason for this disparity is probably that the secondary energies measured in this experiment are lower than the energies expected from the pickup of a neutron or proton by 125-Mev deuterons. The energy of a pickup H^3, for example, should be of the order of the deuteron energy minus the binding energy of the neutron (~10 Mev). This energy (~100 Mev) is well above the energies detectable by this apparatus in the forward direction. Thus in the energy region measured by this apparatus there is presumably some other mechanism that controls the disintegration process.

It seems likely that at these low energies most of the secondary fragments are coming from an evaporation type of process. The most probably primary reactions are (a) deuteron stripping to form excited Li^8 and Be^8 nuclei, (b) inelastic deuteron scattering or deuteron stripping without capture to form excited Li^7 nuclei, and (c) the knock-out of a proton or a neutron to form excited Li^6 or He^6 nuclei. If one lists the possible two-body decays for the above five excited nuclei and gives each of them equal weight, he may expect particles H^1, H^2, H^3, He^3, and He^4 to be in ratios 2, 3, 3, 1, 3 (TableII). These ratios are seen to be in rough agreement with the observed cross sections if one remembers that the proton cross section is increased by the low-energy protons coming from the three primary reactions postulated above.

Table II

The possible two-body decays to stable nuclei by the five excited nuclei, He^6, Li^6, Li^7, Li^8, and Be^8.

Observed Fragment \ Excited Nucleus	He^6	Li^6	Li^7	Li^8	Be^8	Number of Stable Residual Nuclei
H^1	—	—	He^6	—	Li^7	2
H^2	—	He^4	—	He^6	Li^6	3
H^3	H^3	He^3	He^4	—	—	3
He^3	—	H^3	—	—	—	1
He^4	—	H^2	H^3	—	He^4	3

B. The differential Cross Section for the Production of Li^8 Nuclei in the Reaction $H^2 + Li^7 \rightarrow H^1 + Li^8$ by 125-Mev Deuterons

During the scanning of the plates exposed to the disintegration products of lithium (Section III-A), several Li^8 tracks were found that could have come from the above reaction. A systematic search was then instituted to discover a sufficient number of these tracks to measure a differential cross section. In all, 536 Li^8 and 79 B^8 tracks were found on the seven plates scanned. The B^8 nuclei could not have been produced by a deuteron and a lithium nucleus, and therefore must have come from contamination (probably oxygen, see Appendix A) of the lithium target. If the contaminant is oxygen then one may expect, from symmetry considerations, an approximately equal number of Li^8 nuclei appearing as background to the above reaction. This assumption is borne out by the presence, in regions that Li^8 fragments from the expected two-body reaction cannot reach, of Li^8 nuclei in roughly the same abundance as the B^8 nuclei.

The angular distributions of the hammer tracks found on the seven plates are shown in Fig. 12. The regions bracketed by the arrows are those in which Li^8 nuclei from the two-body reaction should appear. The large angular spread on Position 1 is caused by the energy loss in the target of the Li^8 ions. Thus Position 1 observes Li^8 nuclei pro-

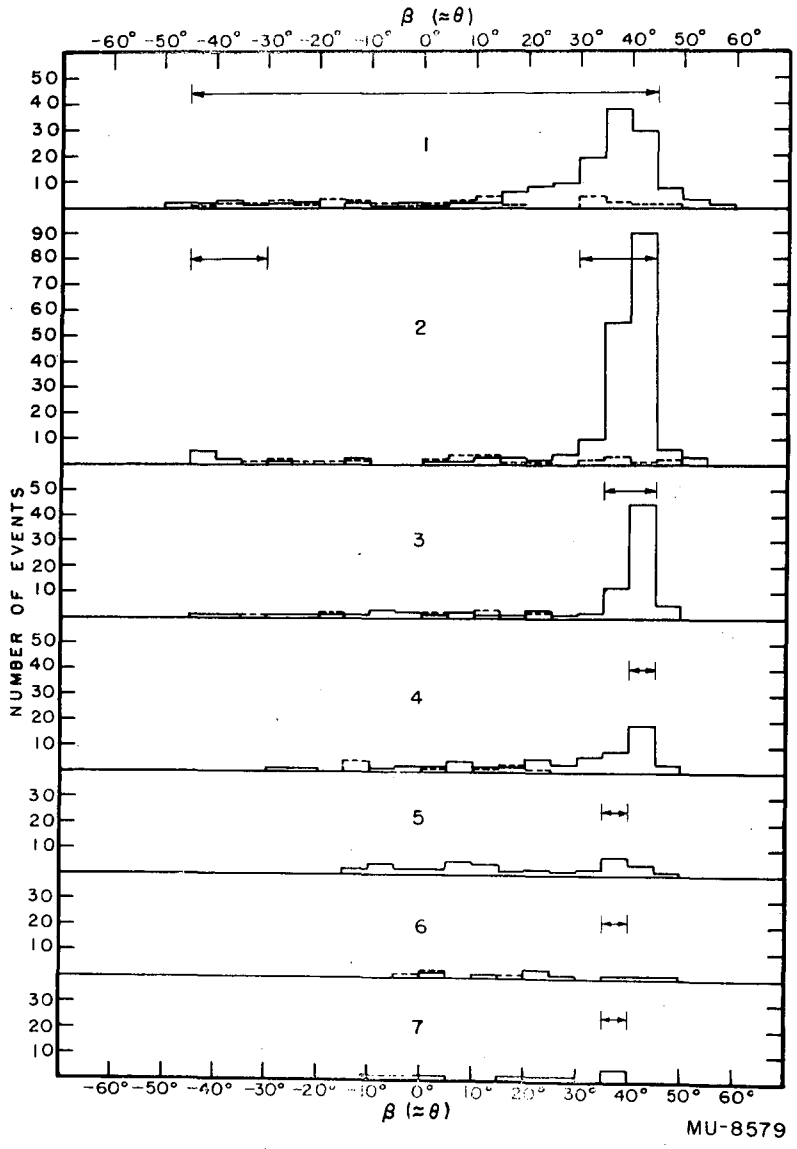

Fig. 12 The number of hammer tracks found in Positions 1 through 7 in 5^{o} intervals from -70^{o} to $+70^{o}$ from the beam directions. The solid lines are Li^{8} nuclei; the dashed lines are B^{8} nuclei. The regions bracketed by the arrows indicate where the Li^{8} nuclei from the two-body reaction: $H^{2} + Li^{7} \rightarrow H^{1} + Li^{8}$, should fall.

duced from 0^{o} to 45^{o} from the beam direction but occuring at corresponding depths in the target. The bunching near 40^{o} is caused by the large ratio of the center-of-mass solid angle to the laboratory solid angle at 41^{o}.

Figure 13 is a cross section of the momentum-angle relationship for the above two-body reaction as seen in the laboratory-system momentum space for deuterons of 125 Mev energy. (Appendix F). The shaded area represents the volume in momentum space into which the Li^{8} fragments are spread by the energy loss in the target; θ is the laboratory angle; θ^{*}, the center-of-mass angle; p, the laboratory momentum; p^{*}, the center-of-mass momentum; and p_{cm}, the momentum given to the Li^{8} by the center-of-mass velocity. If there were no energy loss in the target, the laboratory-system momentum p would fall on the circle. The energy loss, however, has the effect of reducing the magnitude of p and causing it to fall into the shaded area. The vertical swaths numbered 1 through 7 represent the volume of momentum space as seen by the seven plates. The distance x from the target where a Li^{8} fragment is detected (Fig. 3) is given by $x = 2\rho \cos \beta$. Because the momentum p is proportional to ρ and as $\beta \approx \theta$, x is proportional to $p \cos \theta$. Therefore equal intervals in x see equal horizontal intervals in Fig. 13 independent of θ. The quantity that is measured in the emulsions is $\frac{\Delta N}{\Delta \omega \Delta p}$ (Section II-C). To obtain $\frac{\Delta N}{\Delta \omega}$ for the two-body reaction, it is necessary to sum $\sum_{i} \frac{\Delta N_{i}}{\Delta \omega_{i} \Delta p_{i}} \Delta p_{i}$ at a constant θ. For Positions 3 through 7 the effect of the target thickness was neglected and $\frac{\Delta N}{\Delta \omega}$ was obtained merely by multiplying $\frac{\Delta N}{\Delta \omega \Delta p}$ by $\frac{dp}{d\theta} \Delta\theta$, where $\frac{dp}{d\theta}$ is evaluated from the kinetics of the two-body reaction (Appendix F) and $\Delta\theta$ is the angular interval in which the N events were observed. For Positions 1 and 2, account must be taken of the events that are not observed at an angle θ because of the spread in momentum caused by the target. This was accomplished by multiplying $\frac{\Delta N}{\Delta \omega \Delta p}$ by $\frac{dp}{dR} \Delta R_{\theta}$, where $\frac{dp}{dR}$

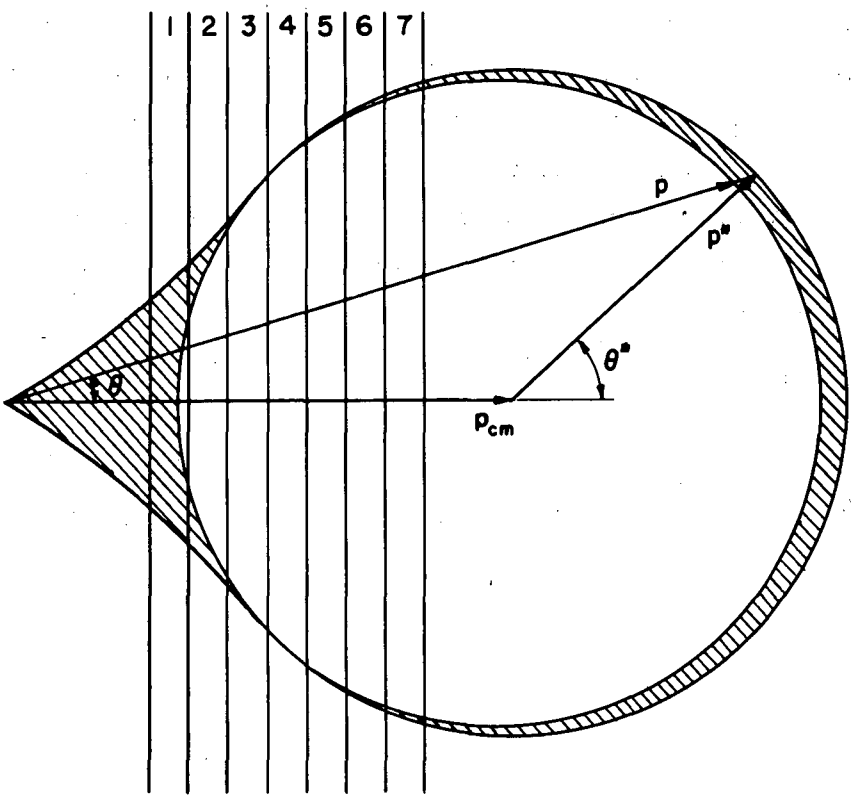

MU-8578

Fig. 13 A cross section of the volume in momentum space occupied by Li^8 nuclei from the reaction Li^7 (d, p) Li^8. (For further discription see text, Section III-B).

is evaluated from the range-energy relationship as measured in Section III-E and ΔR is the thickness of the target as seen at an angle θ. Finally $\frac{\Delta N}{\Delta \omega^*}$ (c.m.) is obtained by multiplying $\frac{\Delta N}{\Delta \omega}$ by $\frac{d\omega}{d\omega^*}$ and by a factor f (near unity) to take account of those Li^8 ions which picked up an electron in the target and whose paths had a larger radius of curvature, and were not detected at the proper position.

Figure 14 shows the differential cross section in the center-of-mass system as measured in this experiment. The background has not been subtracted, but is shown approximately by the dashed line. Because of the high intensity (~5000: 1) of other disintegration fragments present on the plates, the scanning efficiency was reduced to about 70%(as averaged on Position 3 by four different scanners). The measured points on the figure have therefore been increased by a factor of 1.4. The errors on the cross section are statistical, while the horizontal bar indicates the angular range represented by a point. Of the two overlapping points at 150^o, the upper one was measured on Plate 1 and the lower one was measured on Plate 2.

The theory represented in Fig. 14 is that of Bhatia[36] et al., and is given by

$$\frac{d\sigma}{d\omega^*} = \frac{M_p^* M_d^*}{2\pi\hbar^4} \frac{k_p}{k_d} G^2\left(\left|\bar{K}_p - \frac{1}{2}\bar{K}_d\right|\right) \sum_{\ell_n} \frac{\Delta_{\ell_n}}{(2j_i+1)} \left[\left(\frac{\pi}{2kR}\right)^{1/2} J_{\ell_n + 1/2}(kR)\right]^2 , \qquad (7)$$

where

$$G\left(\left|\bar{K}_p - \frac{1}{2}\bar{K}_d\right|\right) = \frac{2(2\pi a)^{1/2}}{a^2 + (k_p - \frac{1}{2}k_d)^2 + 2k_p k_d \sin^2\frac{\theta^*}{2}} ,$$

$$k = \left[(k_d - \frac{M_i}{M_f}k_p)^2 + 4\frac{M_i}{M_f}k_p k_d \sin^2\frac{\theta^*}{2}\right]^{1/2} ,$$

$$M_d^* = \frac{M_d M_i}{M_d + M_i} ,$$

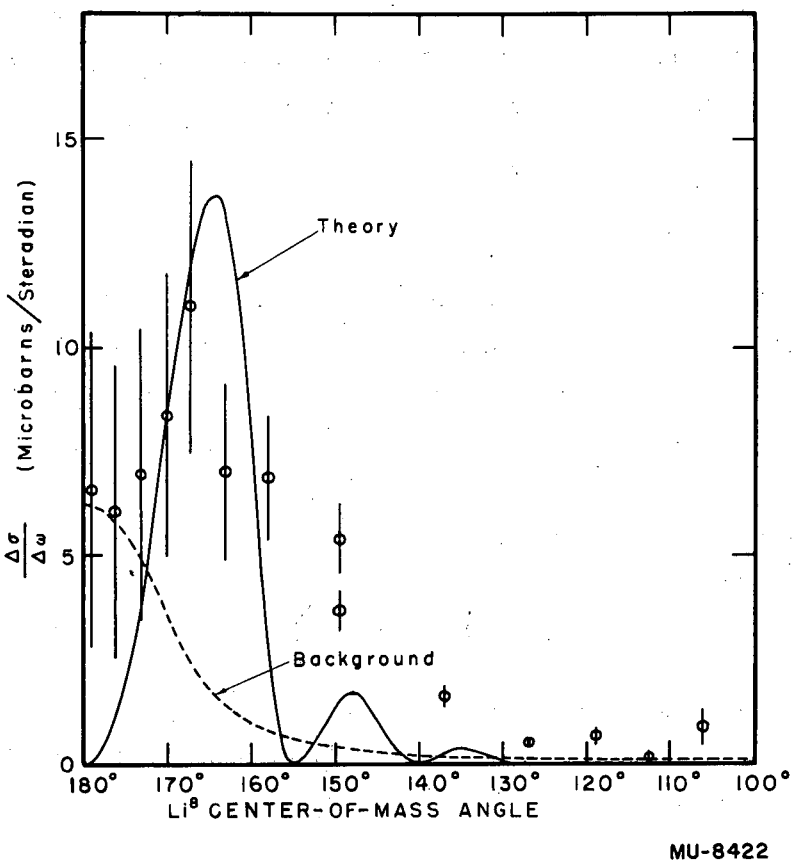

Fig. 14 The measured cross section in the center-of-mass system for the production of Li^8 nuclei from the reaction $H^2 + Li^7 \rightarrow H^1 + Li^8$. The errors shown are statistical only. The dashed curve is a rough estimate of the background, which has not been subtracted from the measured points. The solid curve represents Bhatia's[36] theory for (d, p) reactions.

$$M_p^* = \frac{M_p M_f}{M_p + M_f} ,$$

$$k_d = \frac{M_d^* v_d}{\hbar} , \qquad (v_d \text{ is measured in the laboratory-system})$$

and

$$k_p = \frac{M_p^* v_p}{\hbar} . \qquad (v_p \text{ is measured with respect to the final nucleus})$$

Here i, f, d, and p refer respectively to the initial nucleus, the final nucleus, the deuteron, and the proton. The term α is the coefficient in the exponent in the deuteron wave function

$$\psi = \left(\frac{\alpha}{2\pi}\right)^{1/2} e^{-\alpha r} ,$$

and is approximately 0.23×10^{-13} cm^{-1}. R is a radial parameter, which should correspond to the radius of the nucleus plus the range of nuclear forces. For the curve shown, $R = 7.2 \times 10^{-13}$cm. If Butler's theory[37] is used, $r_o = 5.3 \times 10^{-13}$cm gives a distribution of the same shape but does not predict an absolute cross section. The term ℓ_n is the angular momentum in units of $\hbar$ of the captured neutron. For the curve shown $\ell_n = 1$. If the ground state of Li^7 has spin 3/2 with odd parity, then this predicts that the ground state of Li^8 has spin 3, 2, 1, or 0 with even parity. The expression $\frac{\Lambda_{\ell_n}}{2j_i + 1}$ is proportional to the neutron-capture probability, and was taken to be 6.35×10^{-49} gm^{2}cm^7 sec^{-4}.[38]

The values for the parameters r_o, ℓ_n, and Λ_{ℓ_n} were the same as those used by Holt and Marsham[38] to fit their measurements on the same reaction at a deuteron energy of 8 Mev. The results seem to be consistent with the theory only between 160° and 180°. It should be remarked, however, that the theory has been extrapolated from 8 to 125 Mev, and the fit as to order of magnitude is good. The discrepancy at smaller angles may be attributable to the fact that Bhatia's theory is derived using the Born approximation and does not apply where the interaction between the proton and the nucleus is strong. The high cross section

at smaller angles may therefore be due to compound-nucleus formation with the ejection of a proton.

C. Li^8 The Range Distribution of Alpha Particles Following the Decays of Li^8 and B^8

From a measurement of the range distribution of the alpha tracks (Fig. 15) resulting from the reactions

$$\left.\begin{array}{ll} \text{(a)} & B^8 \rightarrow e^+ + Be^{8*} \\ \text{(b)} & Li^8 \rightarrow e^- + Be^{8*} \end{array}\right\} \rightarrow Be^{8*} \rightarrow 2He^4, \qquad (8)$$

the energy-level structures arising from these mirror processes in the short-lived Be^8 nuclei may be compared. Although the Be^8 from the decay of Li^8 has been studied by many investigators,[39,40,41,42] additional measurements were taken on the alpha particles from Reaction (8b) as a means of calibration of the method and in the hope of improving the statistics over previous investigations. The alpha-particle range distribution from Reaction (8a) was studied for the purposes of (a) checking the similarity of the two mirror nuclei, Li^8 and B^8, and (b) searching for a possible new level in the excited Be^8 nucleus. The probability of a second level is enhanced for reaction (8a) because of the slightly greater energy (~1 Mev) available in the B^8 nucleus than in the Li^8 nucleus.

The hammer tracks found in the search for the two-body reaction (Section III-B) were augmented by hammer tracks taken from plates exposed to a beryllium target bombarded by alpha particles under similar conditions. The Be^8 tracks could be differentiated from the Li^8 tracks by the differences in range and in grain density for a given radius of curvature in the cyclotron magnetic field. Owing to the short range of the Li^8 or B^8 tracks penetrating the emulsion, in about one-third of the decays one of the alpha tracks left the emulsion before the end of its range. In these cases the range of the remaining alpha particle was measured from the end of the B^8 or Li^8 track. In the events in which both alpha particles remained in the emulsion, the two ranges were averaged. The latter cases provided a means for estimating the errors

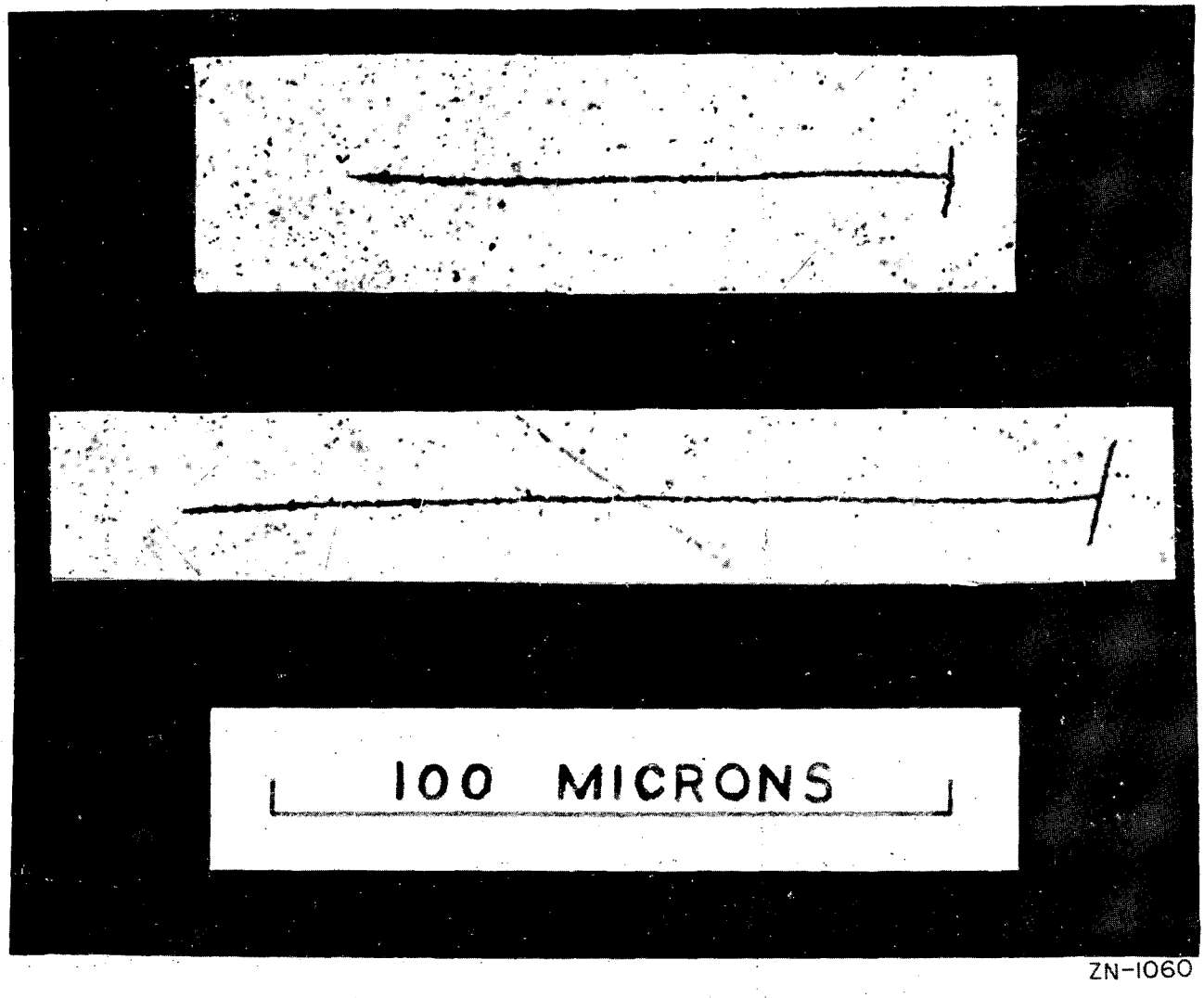

Fig. 15 Photomicrographs of tracks of Li^8 and B^8 nuclei: (Top) a 28-Mev Li^8 track, (Bottom) a 66-Mev B^8 track.

involved in the measurement of the alpha ranges. Since the two alpha particles come apart with equal energies in their center-of-mass system, the difference in their measured ranges gives an estimate of the errors due to range straggle, recoil of the Be^8 nucleus from the beta decay, indeterminacy of the end points, and human error. In this manner the standard deviation in the measurement of individual alpha ranges was estimated to be about 0.5 micron. The alpha energies as a function of range were determined from a range-energy relation for C-2 emulsions worked out by Wilkins.[30]

The alpha ranges from 159 B^8 disintegrations and 1252 Li^8 disintegrations, normalized to 100 for comparison, are shown in Fig. 16. No significant difference is detectable; in particular, no additional long-range alpha particles were found following the decay of B^8. The Li^8 distribution is similar to that found by previous investigators.[40,41,42] The combined 1411 events shown in Fig. 17 have a maximum at about $E_\alpha = 1.5$ Mev and a width at half maximum of $\Delta E_\alpha = 0.8$ Mev. Near resonance the distribution may be fitted by a single resonance theory due to Wheeler[43] as modified for the alpha penetrability by Bonner et al.,[44] where $E_0 = 2.9$ Mev, $\Gamma = 1.2$ Mev, and J, the angular momentum of the excited state of Be^8, is 2. Roughly 15% of the decays, principally the higher energy alpha particles, are not included by this resonance and must be explained by the presence of higher levels in the Be^8 nucleus. It is to be noted that the data may be fitted satisfactorily over the entire energy range of this experiment by the single resonance theory if J is chosen as 4, in agreement with the analysis by Bonner et al.[44]

The presence of the longer-range alpha particles, 15 to 25 microns, from the decay of B^8, and the similarity of the B^8 and Li^8 distributions, suggest that the B^8 beta decay leads to the same energy levels in Be^8 as does the Li^8 beta decay. This is in essential agreement with the interpretation of the positron spectrum of B^8 as measured by Alvarez.[45]

D. The Electron Pickup by Li^8 Ions as a Function of their Velocity

In their passage through the metal targets used in this experiment, the Li^8 ions suffer many collisions in which they either lose or pickup

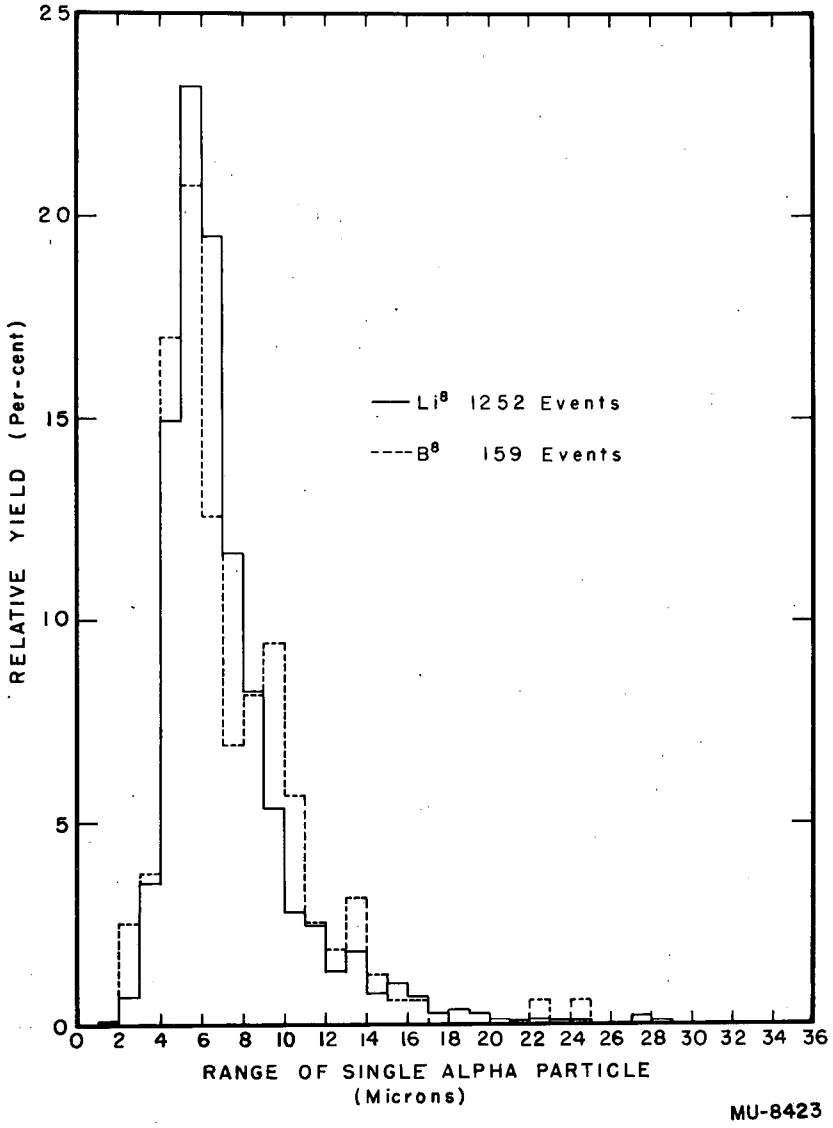

Fig. 16 The distributions of ranges of alpha-particles following the decays of 159 B^8 nuclei and 1252 Li^8 nuclei. Both distributions have been normalized to 100 for comparison purposes.

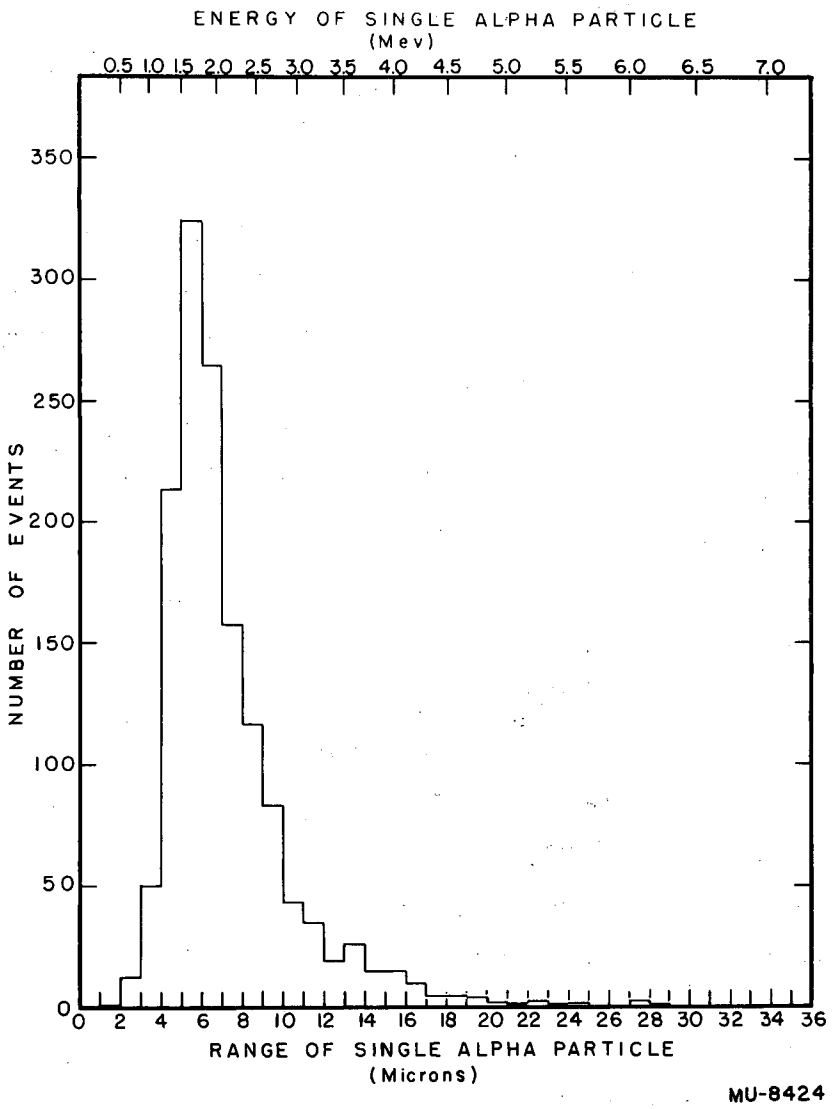

Fig. 17 The combined alpha-particle range distribution following the decays of 1411 Be^8 nuclei.

an orbital electron. When they leave the far side of the target they may be in any one of four charge states (neglecting negative ions). If we denote the fraction of ions carrying charge i by ϕ_i, and the cross section for going from charge i to charge j by σ_{ij}, we obtain three equilibrium conditions:

$$\begin{aligned} &\text{(a)} \quad \phi_0 \sigma_{01} = \phi_1 \sigma_{10} , \\ &\text{(b)} \quad \phi_1 \sigma_{12} = \phi_2 \sigma_{21} , \\ &\text{(c)} \quad \phi_3 \sigma_{32} = \phi_2 \sigma_{23} , \end{aligned} \tag{9}$$

These equations assume that the ions have made many such collisions before leaving the target and that multiple electron transfers are improbable. In the cyclotron magnetic field the radius of curvature of the path of an ion of any given velocity is inversely proportional to its charge. Therefore, by scanning plates whose distances from the target are in the ratios $1/3 : \frac{1}{2} : 1 : \infty$, one can obtain the relative numbers of the various ions as a function of their emission angle, and thus obtain the ratios of the cross sections σ_{ij} as a function of velocity.

In order to improve the statistics on electron capture obtained from the Li^8 ions leaving a lithium target, Li^8 ions were used which came from a beryllium target bombarded by alpha particles, for which process the cross section for Li^8 production seems to be much higher than for deuterons on a lithium target. The geometry of this experiment was such that neutral Li^8 atoms were not collected and the velocities were too high for one to obtain sufficient singly charged Li^8 ions. Therefore only the ratio ϕ_2/ϕ_3 was measured. In Fig. 18 the ratio of double-charged to triple-charged Li^8 ions leaving a lithium and a beryllium target is shown as a function of velocity. The velocity is measured in units qv_o, where $qv_o = qe^2/\hbar$ $(q = 3)$ or 6.56×10^8 cm/sec. The errors shown are statistical only.

The cross section for an ion of charge q to capture an electron from a neutral atom with Z electrons has been estimated by Bohr[46] to be

$$\sigma_c = 4\pi \, a_o^2 \, q^5 \, Z^{\frac{1}{3}} \left(\frac{v_o}{v}\right)^6 , \tag{10}$$

where $a_o = \hbar^2/mc^2$. The cross section for the loss of the above electron can be calculated[46] from the classical theory of ionization to be

$$\sigma_\ell = 4\pi a_o^2 \frac{Z(Z+1)}{q^2} \left(\frac{v_o}{v}\right)^2 \qquad (11)$$

for low-Z materials. The ratio of the two cross sections is shown in Fig. 18 for beryllium oxide and lithium oxide. As no attempt was made to prepare a clean beryllium or lithium target, there was most likely a layer of oxide on the surface, which determined the equilibrium conditions. The charge-exchange cross sections are of the order πa_o^2 ($\sim 10^{-17}$ cm^2) in this region, and equilibrium is established in a distance of the order of angstroms.

More exact calculations have been made for the capture cross sections, classically by Thomas[47], and quantum-mechanically by Brinkman and Kramers[48], Mott and Massey[49], Bates and Dalgarno,[50] and--most recently--by Jackson and Schiff[51]. Of these, Jackson and Schiff obtain the best agreement with experiment; however, they evaluate their theory only for protons in hydrogen. It should be noted that Bohr's estimate of the ratio ϕ_2/ϕ_3 in this region fits the data well, particularly in absolute magnitude. It can not be said, however, that there is a detectable difference between Li_2O and BeO. From these observations it can be concluded that the exponent of the velocity in the capture cross section probably lies between -5 and -8.

E. The Range of Li^8 Nuclei in Emulsion

The range-energy relation for Li^8 nuclei in Ilford C-2 emulsion as determined in this experiment is shown in Fig. 19. All hammer tracks have been included except those clearly identified as B^8. The ranges were measured from Point A to Point B as shown below. Point B is the point

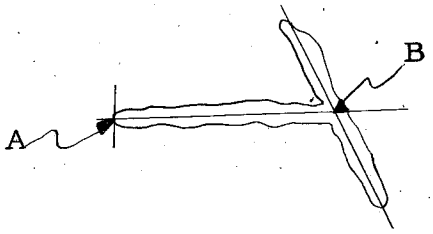

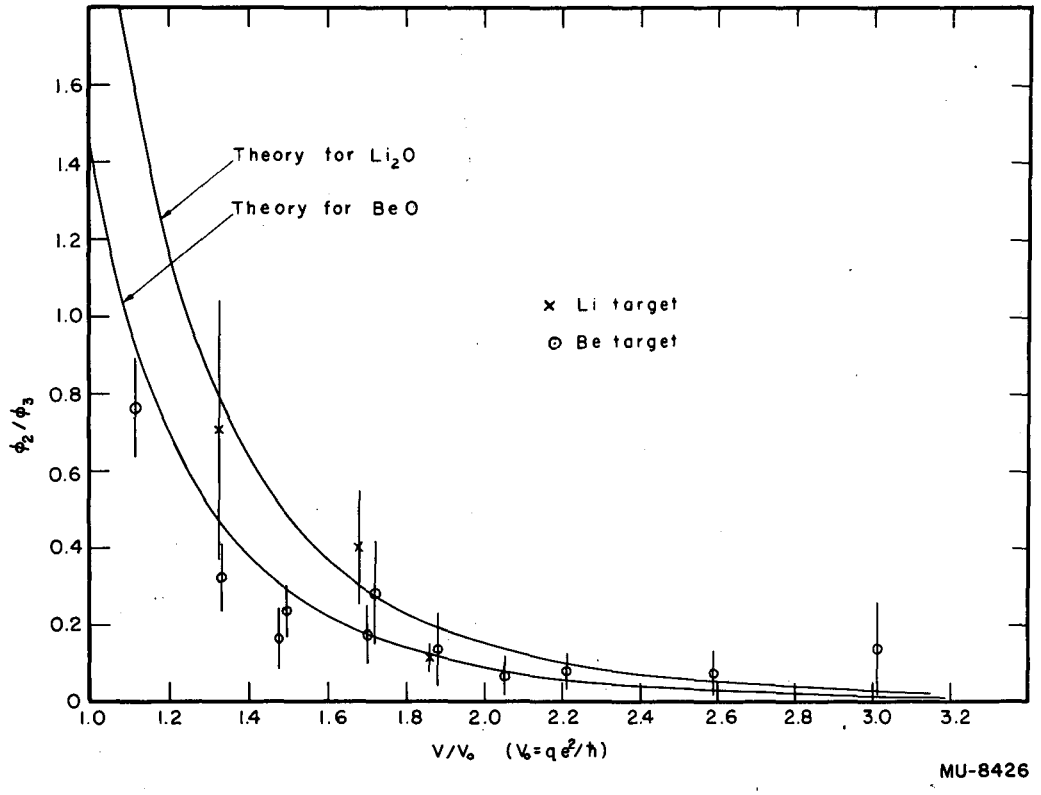

Fig. 18 The measured ratio of double-charged to triple-charged Li^8 ions leaving a lithium target and a beryllium target as a function of their velocity in units qv_o ($q = 3$, $v_o = \frac{e^2}{\hbar}$). The theory represented is that of Bohr[46] for Li_2O and BeO.

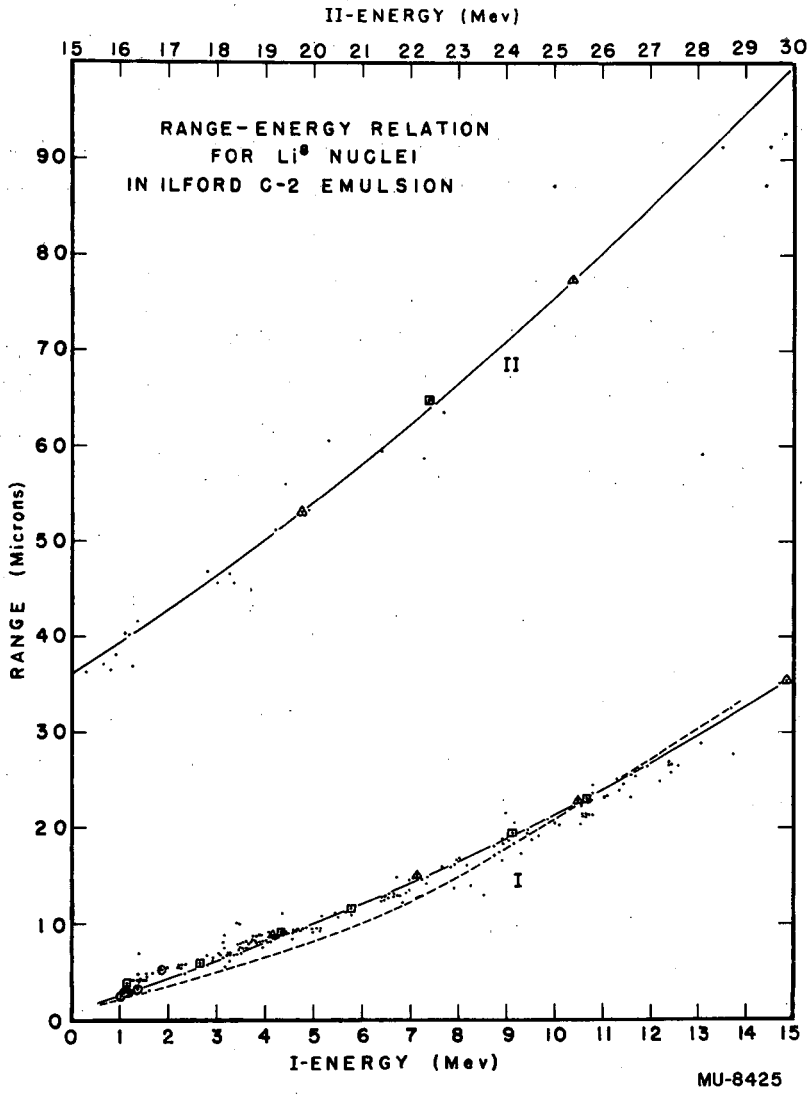

Fig. 19 The range-energy relation for Li^8 nuclei in Ilford C-2 emilsion.

- Li^8 - this experiment
- Li^8 - Barkas
- Li^6 (transformed to Li^8) Neuendorffer
- He^4 (transformed to Li^8) - this experiment
- ——— Wilkins
- – – – Cuer and Longchamp

where the Li^8 disintegrated into two alpha particles (plus an electron and neutrino) and is determined by the intersection of two straight lines; one passed through the Li^8 track and one through the two alpha tracks. Point A is the farthest point from B on the Li^8 track and corresponds approximately to the point where the Li^8 ion entered the emulsion. The energies were determined from the momenta calculated from the $\overline{H\rho}$ (Section II B). In order to minimize the effect on the $\overline{H\rho}$ of errors in measuring the entrance angle β I used tracks with $|\beta| < 30^\circ$ except for the five points of highest energy. Because B^8 ions with four charges have almost the same range as Li^8 ions with three charges there is some contamination of the distribution at low velocities. The points at the lowest energies, however, are from Li^8 with one or two charges and do not suffer from this contamination.

Figure 19 also shows seven points measured by Barkas[52] for Li^8 nuclei in a similar experiment, and five points measured by Neuendorffer et al.[53] for Li^6 nuclei and corrected by the mass ratio to Li^8. Not shown are two points measured by Farragi[54] for Li^7 nuclei, which coincide essentially with Neuendorffer's two lowest points.

Theoretical range-energy relations have been derived by Cuer and Longchamp[55] (dashed curve) and by Wilkins[30] (solid curve). Above 8 Mev, where the effects of electron pickup and of energy loss to the nuclei may be neglected, I have extrapolated Wilkins's lithium curve, using his alpha-particle ranges and the relations (for a derivation of these equations, see Appendix G)

$$\text{(a)} \qquad \frac{q^2 R}{M} = \frac{q_\alpha{}^2 R_\alpha}{M_\alpha} + C \tag{12}$$

and

$$\text{(b)} \qquad \frac{T}{M} = \frac{T_\alpha}{M_\alpha} ,$$

where q, R, M, and T are the charge, range, mass, and energy of a Li^8 nucleus and the subscripts α refer to the corresponding quantities for alpha particles. C is a constant (2.8 microns) chosen to make the extrapolation fit at 8 Mev. I have also measured six points on the alpha-particle range-energy curve, using approximately 20 alphas at each point, and upon transforming them by the above equation I have ob-

tained good agreement with the extrapolation above 8 Mev. This agreement serves as a check on the magnetic-field measurement used to determine the particle energies.

The exact assumptions that went into the derivations of the two theoretical curves below 8 Mev are not given by the different authors.[30,55] Their general approach was the same, however, in that they transformed an empirical alpha-particle range-energy relation to lithium on the basis of assumptions about the charge carried by the lithium ion as a function of velocity. Both derivations[30,55] include the estimates of Knipp and Teller[56] for the mean square charge carried by the ion. Cuer and Longchamp then inserted this charge into the formula of Blackett[57] to obtain their ranges; whereas it appears from Wilkins's discussion that he carried out more careful calculations along the lines of Knipp and Teller.[56]

As can be seen from Fig. 19, the agreement with Wilkins's relation is the best at the lowest velocities, however, Barkas's and my measurements are about one micron longer than those of Farragi and of Neuendorffer et al. (the theoretical curves were normalized to Farragi's measurements at this point). This discrepancy may be due in part to the method of measurement, which is necessarily different for a Li^8 hammer track than for Li^6 and Li^7 tracks. It should be noted that Neuendorffer's highest-energy point coincides with our measurements and disagrees with the theoretical predictions.

I would like to point out that the range $R_L(T_L)$ of any lithium ion of mass M_L and energy T_L may be obtained from this curve by the relation

$$R_L(T_L) = \frac{M_L}{8} R\left(\frac{8}{M_L} T_L\right). \tag{13}$$

IV. OBSERVATIONS

As with all experiments, this one could have been improved in several ways, and I therefore list some possible modifications or lines of attack which seem promising and which should eventually be pursued.

(a) One outstanding problem was the energy limitation on the secondary fragments imposed by the finite size of the cart that enters the cyclotron tank. Higher-energy fragments might be obtained by use of auxiliary probes or extension devices on the cart, or by placing the plate so as to intercept high-momentum fragments before they leave the cart.

(b) The discrimination between H^2 and He^3 and between H^3 and He^4 could probably be improved by gap-counting the ends of the tracks.

(c) The angular distributions could be extended to larger angles by different cart arrangements.

(d) Other targets, other bombarding particles, and other energies should be used in an effort to more accurately describe the disintegration process.

(e) The neutrons leaving the target could be measured by proton recoils in C-2 emulsion or from the reaction Li^6 (n, α) H^3 in Li^6 loaded emulsion.

(f) The study of the electron pickup by heavy ions could be extended to other fragments and to other target materials. An interesting target material would be nuclear emulsion itself. The electron pickup probabilities could then be tied directly to the measured residual ranges and ionizations. Further, the yields of secondary fragments from such a target could be used to analyze previous work done on disintegrations within the emulsion itself.

ACKNOWLEDGMENTS

I am particularly indebted to Dr. Walter H. Barkas for having suggested this research program and for his helpful guidance. I am grateful to Dr. Robert Thornton for his continued interest and support.

I wish to thank Dr. Robert Deutsch and Mr. Evan Bailey for their help, advice and constructive criticism.

Most of the scanning and many of the calculations necessary for this experiment were performed by Mrs. Doreen Hornback, Mrs. Jean Spalding, Mrs. Louise Shaw, Mrs. Jamesine Friend and Mr. John Spalding.

To Mr. Roland Michaelis my sincere gratitude for having processed the many emulsions used in this experiment.

Lastly, I would like to thank the members of the film program, the cyclotron crew, and all the many people whose contributions, large or small, made this work possible.

This work was done under the auspices of the U.S. Atomic Energy Commission.

APPENDICES

A. Target Contamination

Thin metallic lithium targets are very subject to contamination (particularly by oxygen), and although precautions were taken the target used in this experiment did pick up some contamination, as is shown by the presence of 79 B^8 tracks among the 615 hammer tracks found on the seven plates (Section III-B). Since a boron nucleus is not formed from a deuteron and a lithium nucleus, this contamination must come from higher-Z elements.

The lithium target was prepared by rolling a small piece of lithium between steel rollers until it was 0.0024 inch thick as measured by micrometer calipers. (It was necessary to stop rolling at this point because the foil was sticking to the rollers with a force comparable with its tensile strength). During the rolling and subsequent handling the target was kept moist with kerosene until it was placed in the cyclotron air lock and pumped down to cyclotron pressures. Up to this time the foil retained its metallic properties, i.e., flexibility and dark color; upon removal from the air lock after the exposure it was quite brittle and white in appearance. This was due to the formation of lithium oxide when the target came in contact with the air in the air lock after the exposure. The contamination present in the target during the exposure was probably oxygen that had been trapped or combined in the kerosene, and perhaps carbon that remained in the kerosene residue after evaporation in the cyclotron vacuum.

The percentage oxygen (or carbon) contamination may be estimated from the number of B^8 fragments found in the emulsion, and the cross section for their production in oxygen or carbon. These cross sections can be estimated from the experiment by Deutsch,[27] in which he found that about 0.1% of all the fragments from the 375-Mev alpha bombardment of both beryllium and aluminum are B^8 nuclei. Since the total ineleastic cross section in these elements is of the order of 1/2 barn and the average multiplicity is two or three charged particles per disintegration, the total cross section for the production of B^8

should be about a millibarn. The apparent cross section (per lithium atom) for producing B^8 fragments in this experiment is about 10^{-3} millibarn. Therefore the oxygen and carbon contamination should be less than 1% and its effect on the general spallation yield (Section III-A) should be negligible.

Its effect on the yield of Li^8 nuclei from the reaction $H^2 + Li^7 \rightarrow H^1 + Li^8$, however, is considerable because of the small cross section for this reaction ($\sim 10^{-29}$ cm^2), (Section III-B). Since the principal isotopes of oxygen and carbon are symmetric in their numbers of protons and neutrons, the yields of the mirror nuclei, Li^8 and B^8, from these sources should be equal. Therefore the background of Li^8 fragments from this contamination has been estimated from the yield of B^8 fragments (Section III-B).

B. Processing and Care of Emulsions

The nuclear track emulsion used was Ilford C-2 glass-backed emulsion 200 microns thick, 1 inch by 3 inches. The plates were processed after exposure as follows:

Process	Solution	Time	Temperature
Developer	1: 6 Kodak D-19	30 minutes	20°C
Stop bath	H_2O	5 minutes	20°C
Fixer	Kodak acid hardening	5 hours	20°C
Wash	H_2O	2 hours	tap water, uncontrolled
Softener	5% Glycerine	1 hour	room temperature
Dry	Air	1 day	room temperature

The processed plates were stored in wooden boxes with moistened sponges to retard peeling. Care was taken not to rub the surfaces during processing and handling, as this might remove part of the emulsion surface and consequently shorten the measured ranges.

C. Derivation of the Expression for $\overline{H\rho}$.*

The particle motion in the field of the cyclotron is described in terms of cylindrical coordinates (r, ϕ, z) coaxial with the cyclotron field. Consider orbits in the median plane where the magnetic field H has only one component $H_z(r)$. Let (r_1, ϕ_1) be the point of origin (the target) and (r_2, ϕ_2) be the point of detection (the plate). The measurable parameters in this experiment are r_1, r_2, ϕ_1, ϕ_2, and $\beta_2 = \tan^{-1} \frac{1}{r_2}\left(\frac{dr}{d\phi}\right)_2$. The angle β_2 is thus the complement of the angle between the particle trajectory and the radius vector r_2 at the point of detection.

The Lagrangian for the particle motion in the median plane is:

$$L = -m_o c^2 \left(1 - \frac{\dot{r}^2 + r^2 \dot{\phi}^2}{c^2}\right)^{1/2} + \frac{e}{c} \phi \int_{R_1}^{r} r H dr , \qquad (14)$$

where R_1 is the inner libration limit of the particle orbit. Integration of the Lagrangian equation of motion for ϕ yields the quantity

$$\frac{m_o r^2 \dot{\phi}}{\left(1 - \frac{v^2}{c^2}\right)^{1/2}} + \frac{e}{c} \int_{R_1}^{r} r H dr$$

as a constant of the motion; $\dot{r}^2 + r^2 \dot{\phi}^2 = v^2$ is also a constant of the motion. Then if $\tan \beta = \frac{1}{r} \frac{dr}{d\phi}$,

$$r \cos \beta = r_1 \cos \beta_1 - \frac{1}{H\rho} \int_{r_1}^{r} r H dr , \qquad (15)$$

where for the momentum, $m_o v \left(1 + \frac{v^2}{c^2}\right)^{-1/2}$, we have written $\frac{e}{c} \overline{H\rho}$. Since the point of detection also lies on the orbit we have

---

* This derivation is taken from W. H. Barkas, Phys. Rev. 78, 90 (1950) and W. H. Barkas, Meson Mass Measurements I - Theory of the Mass Ratio Method, Report No. UCRL-2327, Sept. 16, 1953

$$\overline{H\rho} = \frac{\int_{r_1}^{r_2} r H \, dr}{r_1 \cos \beta_1 - r_2 \cos \beta_2} . \qquad (16)$$

For a particle whose trajectory makes an angle α with the median plane, the above expression becomes

$$\overline{H\rho} = \frac{\sec \alpha \int_{r_1}^{r_2} r H \, dr}{r_1 \cos \beta_1 - r_2 \cos \beta_2} . \qquad (17)$$

It should be noted that this expression is a good approximation only for orbits lying near the median plane. For the purposes of this experiment, where the field is nearly uniform and the trajectories lie near the median plane, the approximation is good to better than 1%.

D. Derivation of Solid-Angle Jacobian for Magnetic Fields*

In order to obtain the relative number of particles N leaving the target in a solid angle $\Delta\omega$ and in a momentum interval Δp, from the number of particles N found in an area A and angular interval $\Delta\beta$ on the emulsion surface, it is necessary to find a transformation R such that

$$\frac{N}{\Delta\omega \Delta p} = R \frac{N}{A \Delta\beta} . \qquad (18)$$

For this purpose we will choose a right-handed coordinate system (x, y, z) such that the z-axis is parallel to the magnetic field. An ion moving in the magnetic field traverses a spiral path with constant speed. The projection of its path in the x-y plane is a circle of radius $\rho\sqrt{1-\mu^2}$, where μ (= cos α) refers the direction of emission to the z-axis and $\rho = \frac{Pc}{qeH}$. Here P is the particle momentum, c is the velocity of light, qe is the charge on the particle and H is the magnetic field. The angles α and ϕ are defined so that

$$z = r \cos \alpha,$$

$$x = r \sin \alpha \cos \phi,$$

$$y = r \sin \alpha \sin \phi,$$

and $$d\omega = \sin \alpha \, d\alpha \, d\phi,$$

* This derivation is taken from W. H. Barkas, Solid Angle Jacobian for Charged Particles in a Magnetic Field, Report No. UCRL-2126, March 10, 1953.

where $\bar{r}$ is the radius vector to the particle. The three quantities ρ, μ and ϕ at the origin suffice to describe completely the ion path in a uniform field.

The emulsion surface defines a plane for which z is a constant. The coordinates x and y of the point of detection in this plane are given by

$$x = 2\rho\sqrt{1-\mu^2}\,\sin\left(\frac{z}{2\rho\mu}\right)\cos\left(\phi - \frac{z}{2\rho\mu}\right),$$
$$y = 2\rho\sqrt{1-\mu^2}\,\sin\left(\frac{z}{2\rho\mu}\right)\sin\left(\phi - \frac{z}{2\rho\mu}\right). \tag{19}$$

The particle path is characterized by a constant angle α between the orbit and the z-direction, and by the angle $\beta = -\cot\frac{dy}{dx}$ measured at the point of detection. From Eq. (19) $\beta = \phi - \frac{z}{\rho\mu} + \frac{\pi}{2}$. The Jacobian relating x, y, and β with ρ, μ, and ϕ is given by

$$J\left(\frac{x, y, \beta}{\rho, \mu, \phi}\right) = \begin{vmatrix} \frac{\partial x}{\partial \rho} & \frac{\partial x}{\partial \mu} & \frac{\partial x}{\partial \phi} \\ \frac{\partial y}{\partial \rho} & \frac{\partial y}{\partial \mu} & \frac{\partial y}{\partial \phi} \\ \frac{\partial \beta}{\partial \rho} & \frac{\partial \beta}{\partial \mu} & \frac{\partial \beta}{\partial \phi} \end{vmatrix} \tag{20}$$

or

$$J = -\frac{2z}{\mu^2}\,\sin^2\frac{z}{2\rho\mu}. \tag{21}$$

For this experiment $y = 0$ (Fig. 3), and in terms of the measurable quantities x, z, and β,

$$J = \frac{2}{z}\left[x^2\left(\frac{\pi}{2} - \beta\right)^2 + z^2\cos^2\beta\right]. \tag{22}$$

From this Jacobian we obtain

$$\Delta x\,\Delta y\,\Delta\beta = J\,\Delta\rho\,\Delta\mu\,\Delta\phi.$$

Since $\Delta x\,\Delta y = A$, $\Delta\mu\,\Delta\phi = \Delta\omega$, and $\Delta\rho = \frac{c}{eH}\Delta p$,

we obtain

$$\frac{N}{\Delta\omega\Delta p} = \left(J\frac{c}{qeH}\right)\frac{N}{A\,\Delta\beta} \quad . \tag{23}$$

The expression for R then becomes

$$R = \frac{2zc\cos^2\beta}{qeH}\left[1 + \frac{x^2\left(\frac{\pi}{2} - \beta\right)^2}{z^2\cos^2\beta}\right] . \tag{24}$$

E. The Energy and Angular Indeterminacy of the Incident Deuterons

The circulating deuterons in the magnetic field of the cyclotron, where they pass through a vertical line a distance r from the center, are not well defined either in energy or direction. This indeterminacy arises from the presence in the beam of sizable radial and vertical oscillations. These oscillations may be caused by many factors, some of the more important being (a) a discrepancy (the order of 1-1/2 inches*) between the geometric and magnetic centers of the cyclotron, (b) the finite size of the ion source and (c) inhomogeneities in the magnetic field. Moreover the presence of the target itself changes the character of the beam in two distinct ways. A thick target clips the beam so that the particles are intercepted at their outer libration limits. This yields a unidirectional flux of particle (the orbits are tangential to concentric circles at their libration limits); the energies, however, are spread out so that they lie below the nominal energy for that radius. A thin target, on the other hand, does not stop the particles; and if the multiple scattering is not too great, a single particle may traverse the target many times.[58] This may cause both the energy and the direction of the incident deuterons to deviate from their nominal values (the energy of a deuteron with a radius of 65 in. in the cyclotron field is 130 Mev).

A measure of the angular divergence of the deuterons striking a 0.0024-inch lithium target can be obtained from the angular spread of the Li^8 nuclei, of a given momentum, from the reaction $Li^7(d,p)Li^8$. It may be seen from Fig. 13 that the effect on the angle ϕ (between the deuteron and the Li^8 nucleus) of the energy loss in the target is negligi-

ble at Position 4. The effect of the energy spread of the incident deuterons may also be neglected in this position since the effect of a small energy change of the deuteron is to change linearly all the magnitudes of the momenta shown in Fig. 13, but to preserve their relative directions. This is a good approximation to the extent that the Q value (-0.20 Mev) may be neglected with respect to the energy of the Li^8 nucleus (~10 Mev) and that the deuteron energy spread be small compared with the deuteron energy (~125 Mev).

The Li^8 nuclei should enter the plate in Position 4 at an angle β (the horizontal projection of θ) of 40.9°. They are actually found to enter mainly between 38° and 43°. This gives a median of 40.5° (the plate was not positioned to better than a degree) with a spread of ± 2-1/2°. Part of this spread (±1°) is due to errors in measuring the entrance angle of the Li^8 fragment and part (±1/2°) to the finite area scanned on the plate. The multiple scattering in the target for one traversal may be neglected at these energies, so that approximately 2°, $\left(\sqrt{(2-1/2)^2 - (1)^2 - (1/2)^2}\right)$, is attributed to the divergence of the beam. This angular spread may be explained by the presence of radial oscillations of about 2 inches at a deuteron radius of 65 inches. This corresponds to an energy variation in the nominally 130-Mev deuterons of about 10 Mev. Since the particles are first intercepted at their outer libration limit, this effect will in general reduce the mean energy of the deuterons striking the target. Therefore I have assumed a mean energy of 125 ± 10 Mev.

F. The Kinetics of the Reaction Li^7 (d, p) Li^8

In order to obtain the momentum-angle relationships used in Section III-B for the Li^7 (d, p) Li^8 reaction as illustrated in Fig. 13, I use a coordinate system (x, y, z) such that the y-axis is parallel to the deuteron direction (Fig. 3). The subscripts 1, 2, 7, and 8 refer respectively to the H^1, H^2, Li^7, and Li^8 nuclei. The angle with respect to the y-axis I designate by θ. Thus energy conservation yields the equation

$$E_2 + E_7 = E_1 + E_8 . \qquad (25)$$

* W. Stubbins - private communication

E is the total energy of a particle in the laboratory-system and is given by

$$E = \sqrt{p^2 c^2 + m^2 c^4} \quad , \tag{26}$$

where c is the velocity of light and m and p are respectively the rest mass and laboratory momentum of the particle. Momentum conservation in the y-direction gives

$$p_2 = p_1 \cos \theta_1 + p_8 \cos \theta_8 \tag{27}$$

and in the plane of the reaction perpendicular to the y-direction gives

$$p_1 \sin \theta_1 = p_8 \sin \theta_8 \quad . \tag{28}$$

In this experiment $p_7 = 0$ and the energy of the Li^8 is low enough to use the classical approximation $E_8 = m_8 c^2 + \frac{p_8^2}{2 m_8}$. Equation (25) then yields

$$T_2 = T_1 + \frac{p_8^2}{2 m_8} - (m_2 + m_7 - m_1 - m_8) c^2 \quad , \tag{29}$$

where T is the laboratory kinetic energy ($T = E - m c^2$).

The term $(m_2 + m_7 - m_1 - m_8) c^2$ is the "Q-value" of this reaction (-0.20 Mev) and may be neglected with respect to the kinetic energy available in the center-of-mass system (~100 Mev). Combining Eqs. (26), (27), (28), and (29) and neglecting terms of order $\frac{p_8}{2 m_8 c}$ with respect to one, and neglecting Q, we obtain

$$\cos \theta_8 = a p_8 + \frac{b}{p_8} \quad , \tag{30}$$

where

$$a = \frac{m_8 + m_1 - m_2}{2 m_8 p_2} + \frac{\sqrt{p_2^2 c^2 + m_2^2 c^4}}{2 p_2 m_8 c^2}$$

and

$$b = -\frac{(m_2 - m_1) m_2 c^2}{p_2} + \frac{(m_2 - m_1) \sqrt{p_2^2 c^2 + m_2^2 c^4}}{p_2}$$

For 125-Mev deuterons $a = 8.20 \times 10^{-4} \left(\frac{Mev}{c}\right)^{-1}$ and $b = 168 \left(\frac{Mev}{c}\right)$.

If the plane of the reaction is taken as the x-y plane then Eq. (6) is the equation of a circle in momentum space

$$\left(p_x - \frac{1}{2a}\right)^2 + p_y^2 = \left(\frac{1}{2a}\right)^2 - \frac{b}{a} . \tag{31}$$

This relation is shown is Fig. 13.

The laboratory and center-of-mass angles of the Li^8 fragments may be obtained from a figure of this type for any given laboratory momentum.

G. Derivation of the Range Transformation Equations*

For this derivation (Eq. (12) in text) it is assumed that an ion of charge qe, moving with velocity v, loses energy at the rate[59]

$$\frac{dT}{dR} = q^2 f(\beta), \tag{32}$$

where T is the kinetic energy of the ion, R is its residual range in microns, and $\beta = v/c$. Since T/M is a function solely of the velocity, M being the ionic atomic weight, Eq. (32) can be written

$$q(\beta)\, d\beta = \frac{q^2}{M}\, dR, \tag{33}$$

with $q(\beta)$ a function of the velocity alone. When the nucleus is moving with a sufficiently high velocity, one assumes that it is completely stripped so that the charge is not a function of the velocity. In a range interval where this condition holds, one may integrate Eq. (33) and obtain

$$\int_{\beta_o}^{\beta} q(\beta)\, d\beta = G(\beta) - G(\beta_o) = \frac{q^2 R}{M} - \frac{q^2 R_o}{M} . \tag{34}$$

---

* This derivation is taken from W. H. Barkas, "The Range Correction for Electron Pickup", Report No. UCRL-1937, August 29, 1952

In this expression $\beta_o c$ is some lower velocity still sufficiently high that the nucleus remains stripped and R_o is the corresponding range. Thus for $\beta > \beta_o$ one can write

$$\frac{q^2 R}{M} = G(\beta) + B_q . \tag{35}$$

The term B_q is a function of the element and is a measure of the range extension caused by electron pickup. Barkas has derived a theoretical expression[52] for B_q as a function of q:

$$B_q = a q^3 , \tag{36}$$

where a is a constant which he evaluated from empirical range-energy relations to be 0.12 microns.

For the transformation from an alpha range-energy curve to a Li^8 range-energy curve, as done in Section III-E, I used C = 2.8 microns. This is consistent with Barkas's predicted value of 2.3 microns $(B_3 - B_2)$.

REFERENCES

1. W. Barkas and J. Bowker, Phys. Rev. 87, 207 (1952)

2. B. B. Cunningham, H. H. Hopkins, M. Lindner, D. R. Miller, P. R. O'Connor, I. Perlman, G. T. Seaborg, and R. C. Thompson, Phys. Rev. 72, 739 (1947)

3. D. R. Miller, R. C. Thompson, and B. B. Cunningham, Phys. Rev. 74, 347 (1948)

4. H. H. Hopkins, Phys. Rev. 77, 717 (1950)

5. F. O. Bartell, A. C. Helmholz, S. D. Softky, and D. B. Stewart, Phys. Rev. 80, 1006 (1950)

6. R. E. Batzel, D. R. Miller, and G. T. Seaborg, Phys. Rev. 84, 671 (1951)

7. J. B. Harding, S. Lattimore, and D. H. Perkins, Proc. Roy. Soc. A 196, 325 (1949)

8. R. H. Brown, V. Camerini, P. H. Fowler, H. Heitler, D. T. King, and C. F. Powell, Phil. Mag. 40, 862 (1949)

9. N. Page, Proc. Phys. Soc., A 63, 250 (1950)

10. H. L. Bradt and N. F. Kaplon, Phys. Rev. 78, 680 (1950)

11. D. H. Perkins, Phil. Mag. 41, 138 (1950)

12. G. Bernardini, G. Cortini and A. Manfredini, Phys. Rev. 79, 952 (1950)

13. U. Camerini, J. H. Davies, P. H. Fowler, C. Franzinetti, W. O. Lock, D. H. Perkins, and G. Yekeutieli, Phil. Mag. 42, 1241 (1951)

14. U. Camerini, P. H. Fowler, W. O. Lock, and H. Muirhead, Phil. Mag. 41, 413 (1950)

15. U. Camerini, W. O. Lock, and D. H. Perkins, Progress in Cosmic Ray Physics, Amsterdam, North Holland Publishing Company (1952)

16. E. Gardner and V. Peterson, Phys. Rev. 75, 379 (1949)

17. E. Gardner, Phys. Rev. 75, 379 (1949)

18. G. Bernardini, E. T. Booth and S. J. Lindenbaum, Phys. Rev. 85, 826 (1952)

19. R. Serber, Phys. Rev. 72, 1114 (1947)

20. M. L Goldberger, Phys. Rev. 74, 1269 (1948)

21. G. Bernardini, E. Booth, and S. Lindenbaum, Phys. Rev. 88, 1017 (1951)

22. V. Weisskoff, Phys. Rev. 52, 295 (1937)

23. H. A. Bethe, Revs. Modern Phys. 9, 69 (1937)

24. E. Bagge, Physik. Z. 44, 461 (1943)

25. K. J. Le Couteur, Proc. Phys. Soc. A63, 259 (1950)

26. W. Barkas and H. Tyren, Phys. Rev. 89, 1 (1953)

27. R. W. Deutsch, Phys. Rev. 90, 499 (1953)

28. R. W. Deutsch, "Yields of Low-Energy Protons and Alphas Resulting from High-Energy Bombardment of Ag", University of California Radiation Laboratory Report No. UCRL-2285, August 5, 1953

29. W. H. Barkas, Phys. Rev. 89, 1019 (1953)

30. J. J. Wilkins, Range Energy Relations for Ilford Emulsions, Report A. E. R. E. -G/R-664, Harwell (1951)

31. W. H. Barkas, Phys. Rev. 78, 90 (1950)

32. F. M. Smith, "Meson Mass Measurements II-On the Measurement of the Masses of Charged Pions", University of California Radiation Laboratory Report No. UCRL-2371, February 2, 1954

33. W. H. Barkas, "Note on Coordinate Transformations and Solid-Angle Jacobian for Charged Particles in a Magnetic Field", University of California Radiation Laboratory Report No. UCRL-2126, March 10, 1953

34 W. H. Barkas and D. M. Young, "Emulsion Tables I-Heavy-Particle Functions", University of California Radiation Laboratory Report No. UCRL-2579 (Rev), September, 1954

35. B. H. Bransden, Proc. Phys. Soc. A 65, 738 (1952)

36. A. B. Bhatia, K. Huang, R. Huby, and H. C. Newns, Phil. Mag. 43, 485 (1952)

37. S. T. Butler, Proc. Roy. Soc. A 208, 559 (1951)

38. J. R. Holt and T. N. Marsham, Proc. Phys. Soc. A 66, 1032 (1953)

39. F.C. Gilbert, Phys. Rev. 93, 499 (1954)

40. F. Ajzenberg and T. Lauritsen, Revs. Modern Phys. 24, 336 (1952)

41. C.M. Class and S.S. Hanna, Phys. Rev. 89, 877 (1953)

42. D. St. P. Bunbury, Phys. Rev. 90, 1121 (1953)

43. J.A. Wheeler, Phys. Rev. 59, 27 (1941)

44. Bonner, Evans, Malich, and Risser, Phys. Rev. 73, 885 (1948)

45. L. Alvarez, Phys. Rev. 80, 519 (1950)

46. N. Bohr, Kgl. Danske Videnskab. Selskab, Mat-fys. Medd. 18, 8 (1948)

47. L.H. Thomas, Proc. Roy. Soc. 114, 561 (1927)

48. H.C. Brinkman and H.A. Kramer, Proc. Acad. Sci. Amsterdam 33, 973 (1930)

49. N.F. Mott and H.S.W. Massey, The Theory of Atomic Collisions, Oxford University Press, New York, 1949

50. D.R. Bates and A. Dalgarno, Proc. Phys. Soc. A65, 919 (1952)

51. J.D. Jackson and H. Schiff, Phys. Rev. 89, 359 (1953)

52. W.H. Barkas, "The Range Correction for Electron Pickup," University of California Radiation Laboratory Report No. UCRL-1937, August 29, 1952

53. Neuendorffer, Inglis and Hanna, Phys. Rev. 82, 75 (1951)

54. H. Farragi, Thesis, Paris 1950

55. P. Cuer and J. Longchamp, Compt. rend. 232, 1824 (1951)

56. J. Knipp and E. Teller, Phys. Rev. 59, 659 (1941)

57. P.M.S. Blackett, Proc. Roy. Soc. 103, 62 (1923)

58. W.J. Knox, "Multiple Traversals of High Energy Particles in a Cyclotron Beam through Thin Targets," University of California Radiation Laboratory Report No. UCRL-883, September 1, 1950

59. M.S. Livingston and H.A. Bethe, Revs. Modern Phys. 9, 245 (1937)